C.1

COLUMNAR TO EQUIAXED TRANSITION IN TIN-LEAD ALLOYS

by

RAMA BALLAV MAHAPATRA

Indian Institute Of Technology , Kharagpur,1981

A THESIS SUBMITTED IN PARTIAL FULFILMENT OF

THE REQUIREMENTS FOR THE DEGREE OF

MASTER OF APPLIED SCIENCE

in

THE FACULTY OF GRADUATE STUDIES

Department Of Metallurgical Engineering

We accept this thesis as conforming

to the required standard

THE UNIVERSITY OF BRITISH COLUMBIA

October 1985

In presenting this thesis in partial fulfilment of the requirements for an advanced degree at the University of British Columbia, I agree that the Library shall make it freely available for reference and study. I further agree that permission for extensive copying of this thesis for scholarly purposes may be granted by the head of my department or by his or her representatives. It is understood that copying or publication of this thesis for financial gain shall not be allowed without my written permission.

Department of Metallurgical Engg.

The University of British Columbia
2075 Wesbrook Place
Vancouver, Canada
V6T 1W5

Date 9 Apr 1986

Abstract

The columnar to equiaxed transition has been examined experimentally in lead-tin alloys. The effect of thermal conditions during solidification, melt superheat, and alloy composition on the transition have been considered. In directionally solidified alloys, the position at which the transition occured was dependent on the temperature distribution in the system, occuring when a specific low temperature gradient was reached at the advancing interface. Melt superheat did not influence the transition position. The alloy content affected the transition position, the transition occuring earlier at higher alloy contents. Adding particles to the melt did not change the position of the transition.

Table of Contents

List of Figures

List of Tables

List of Symbols

CET	Columnar to equiaxed transition
C_o	Initial composition (wt%)
C_L, C_L^*	Liquid composition
C_m	Effective specific heat Cal/gm°C
C_p	Specific heat Cal/gm°C
C_1	Specific heat in liquid/solid state Cal/gm°C
C_2	Specific heat in liquid/solid region Cal/gm°C
ΔC	Concentration difference
D	Diffusion coefficient cm^2/sec
f_s	Fraction solid
f_l	Fraction liquid
df_s	Infinitesimal fraction solid
G	Temperature gradient °C/cm
H	Heat transfer coefficient $Cal/cm^2°Csec$
k	Partition coefficient
K	Thermal conductivity Cal/cm°Csec
L	Latent heat of solidification Cal/gm
N_o	No. of nucleation sites per unit volume
q	Heat flux Cal/sec
R	Lateral growth rate of dendrite cm/sec
s/l	Solid/Liquid
t	Time sec
T_L	Liquidus temperature °C
T_s	Solidus temperature °C
T_o	Initial temperature °C
T_1	Temperature of a node before a time step °C

T_2	Temperature of a node after a time step °C
T_3	Corrected temperature °C
T_a	Ambient temperature °C
ΔT	Supercooling °C
V	Volume of the node cm^3
ρ	Density gm/cm^3

Acknowledgement

I wish to express my sincre gratitude to Dr. Fred Weinberg for his useful advice and guidance throughout the course of this study.

Thanks are also extended to my fellow graduate students for their voluntary assistance and co-operation.

I am also grateful to NSERC Canada for providing financial assistance.

1. INTRODUCTION

1.1 GENERAL REVIEW

Macrostructure in any casting can often be divided into three zones[1] given below. This is shown in Fig 1.

i) Chill zone

ii) Columnar zone

iii) Equiaxed zone

The chill zone consists of fine equiaxed grains having random orientation adjacent to the mould wall. These grains initially nucleate in a thin layer of liquid metal adjacent to the mould wall which is thermally supercooled. The origin and development of the chill zone is fairly well understood.[1-5] Mould wall temperature, thermal properties of the melt etc. are important factors in the formation of the chill zone. The growth of the columnar zone is quite well understood.[1,2,6] The columnar zone consists of large oriented grains which are formed by progressive solidification from the chill zone towards the centre of the casting. The solidification is generally dendritic and the preferred orientation is usually along the <100> direction. The progressive growth of the columnar grains is controlled by the extraction of heat through the solid shell and the mould wall.[7]

The central equiaxed zone consists of large equiaxed grains which are generally dendritic and randomly oriented.

The formation of this zone requires a transition to occur from columnar growth to equixed growth which is the subject of the present investigation.

The ratio of columnar zone to equiaxed zone in a casting is a major factor in determining the properties of as cast materials.[8] For instance a higher fraction of columnar dendrites would make a continuously cast billet more sensitive to cracking.[9] In practice one would like to control the solidification to produce either a wholly equiaxed structure for isotropic properties or a wholly columnar structure to produce anisotropic properties. Therefore it is very important to study the columnar to equiaxed transition in castings in order to be able to control the structure during solidification.

1.2 PREVIOUS WORK

The presence of the central equiaxed zone in a casting has been considered for many years and a number of mechanisms have been proposed to account for the presence of this zone and hence the transition from the columnar to the equiaxed zone.[7,10-21] These mechanisms primarily propose a number of ways in which nuclei can be produced because of crystal multiplication during solidification leading to the growth of equiaxed grains.

1.2.1 COLUMNAR TO EQUIAXED TRANSITION BASED ON CONSTITUTIONAL SUPERCOOLING

In 1953 Winegard and Chalmers[10] suggested a mechanism of columnar to equiaxed transition, (CET) based on the concept of constitutional supercooling. They suggested that the central region of any casting is constitutionally supercooled[22,23] due to the rejection of solute at the advancing columnar interface. This is shown in Fig 2. Therefore equiaxed grains can nucleate in the region which is constitutionally supercooled and form the central equiaxed zone. The sequence of events in the formation of the central equiaxed zone is shown in Fig 3. There have been objections to this mechanism.[16,19] It has been pointed out by Hunt[19] that during dendritic solidification, there is no long range solute build up ahead of the columnar dendritic front. The enriched solute layer is usually of the order of a few microns. This is because the solute rejected is segregated laterally between the dendrites. Therefore the conditions ahead of the advancing columnar interface are not favourable for constitutional supercooling.

1.2.2 BIG BANG MECHANISM

In 1963 Chalmer's[11] proposed another mechanism on CET which is commonly called the Big-Bang mechanism. He performed a series of experiments on Al-Cu alloys to examine the length of the columnar zone as a function of pouring temperature and solute content of the alloy. He observed

that the columnar zone length is increased with an increase in pouring temperature of the melt and is decreased with an increase in solute content of the alloy.[24] Based on the experimental evidence Chalmers proposed that the nuclei which form the equiaxed zone are produced when the hot metal initially contacts the mould wall. Adjacent to the mould wall, a thin layer of liquid metal is thermally supercooled, which results in nucleation of chilled crystals. Some of these crystals can drift to the centre of the melt due to turbulence in the melt. These nuclei would grow to form the central equiaxed zone.[14,15,18] He observed that with an increase in pouring temperature, the columnar zone length is increased. He explained this observation based on the fact that, with an increase in pouring temperature, the chilled crystals which drift to the centre of the melt cannot survive. Therefore the central equiaxed zone is reduced and the columnar zone length is increased.

1.2.3 DENDRITE ARM REMELTING MECHANISM

In 1966 Jackson et al[12] proposed another mechanism for the origin of the equiaxed grains. Microscopic observations on alloys of organic material have shown that dendrite arms can melt off under normal conditions of solidification. Based on this observation, Jackson et al suggested that the same phenomena can take place in metallic systems. Schaefer et al[25] have observed dendrite arm remelting in metallic systems like Sn-Bi and Sn-Cu. A dendrite is a tree like

structure having a primary stalk with secondary and tertiary branches. During dendritic solidification, there is a solute build up around the primary stalk. When a secondary dendrite arm starts growing, it has to go through the solute rich environment before contacting the bulk liquid. During the initial stages, the growth is hindered because of the enriched solute layer. Outside of the solute layer, the secondary dendrite can grow more rapidly. This leads to the formation of a neck at the junction between the secondary and the primary dendrite and also between the tertiary and secondary dendrites. This is shown in Fig 4. Since these junctions are enriched with solute, the melting point is lowered. Due to thermal fluctuations in the melt, the secondary and tertiary dendrite arms can melt off from primary and secondary branches respectively.

In the presence of convection in the melt, the detached dendrite arms are carried to the central region of the casting. Jackson et al[12] suggested that the remelted dendrite arms would grow and form the central equiaxed zone. The presence of convection in the melt is essential for this mechanism to operate. It has been observed that enhancement of convection in the melt with electromagnetic stirring, oscillation of the mould. results in a larger equiaxed zone.[26-30] Electromagnetic stirring during continuous casting reduces the columnar zone length.[31] Similarly it has been observed that by supressing convection in the melt under the application of a magnetic field, or by rotating

the mould, results in a larger columnar zone.[32,33] All the above mentioned observations further strengthen the mechanism of dendrite arm remelting as proposed by Jackson et al. Experiments conducted by Ohno[17] have supported this mechanism.

1.2.4 SHOWERING OF DENDRITES

This theory was proposed in 1967 by Southin.[13] He observed that during ingot solidification the top surface of the ingot loses heat by radiation and convection. This results in the freezing of the top surface. There is dendritic growth from the top surface downward into the ingot. The dendrite and dendrite arms can dislodge from the top surface and sink downward to the centre of the ingot because of gravity or convection (centre of the ingot remains hotter than the top surface). The detached dendrite arms eventually form the central equiaxed zone. Southin conducted an experiment in which a horizontal barrier was placed in the mould thus dividing the mould into two compartments. The barrier did not interfere with the normal pouring conditions. He observed the presence of an equiaxed zone above the barrier and absence below the barrier. He explained this by saying that an equiaxed zone was present in the top compartment, because all the dendrite arms which showered down were trapped in the top compartment and thus could not enter the bottom compartment. This resulted in the absence of an equiaxed zone in the bottom compartment.

Southin also conducted experiments using hot topped ingots. He observed that the columnar zone length in hot topped ingots was larger than the ingots without hot tops. His explanation was that hot topping inhibit the freezing of the top surface. However Cole et al[26] have proposed that, in hot topped ingots natural convection is reduced, thus leading to a larger columnar zone.

All the above mentioned mechanisms have concerned themselves with the formation of nuclei in various ways. These nuclei would grow to form the central equiaxed zone and eventually impede the columnar dendritic front, thus resulting in a columnar to equiaxed transition.

1.2.5 DENDRITE TIP SUPERCOOLING MECHANISM

This mechanism on CET (columnar to equiaxed transition) was suggested by Hunt[19] based on dendrite tip supercooling. Hunt rejected the presence of constitutional supercooling ahead of the columnar dendritic front. Burden and Hunt[34] have experimentally measured the temperature at the tip of the dendrite during directional solidification of Cu-Al alloys. Cu-Al alloys were grown directionally and the metal temperature at a point was measured with a thermocouple. After the columnar dendritic front crossed the thermocouple, the sample was quenched. The temperature of the dendrite tip was then determined by estimating the time at which the interface was at the thermocouple position from the growth velocity and position of the quenched interface. The time

thus determined gave the dendrite tip temperature from the cooling curve as shown in Fig 5(b). The dendrite tip temperature thus determined, as a function of growth velocities and temperature gradients, is shown in Fig 6. The dendrite tip supercooling for various growth rates and temperature gradients is shown in Fig 7. Burden and Hunt have empirically determined[35] the dendrite tip supercooling as a function of the solidification variables. It is given by,

$$\Delta T_c = \frac{GD}{V} + A'(C_o V)^n \qquad 1$$

where ΔT_c = Dendrite tip supercooling °C

G= Temperature gradient °C/cm

V= Growth velocity cm/sec

D= Diffusion coefficient cm^2/sec

C_o = Solute content

A'= Constant

n= (0.4-.05)

At high temperature gradients and low velocities,

$$\Delta T_c = \frac{GD}{V} \qquad 2$$

At low temperature gradients and high velocities

$$\Delta T_c \; a \; V^n \qquad 3$$

Hunt's concept of CET is based on the supercooling at the dendrite tip.[7,18] The dendrite tip temperature is lower than the equilibrium liquidus temperature of the bulk alloy.

Therefore the liquid metal ahead of the columnar dendritic front is thermally supercooled. This is shown in Fig 8. Equiaxed grains can nucleate and grow in the thermally supercooled region. Hunt has derived an expression to predict the type of growth in a casting (columnar or equiaxed) as a function of temperature gradient, dendrite tip supercooling, and number of nucleation sites in the melt.

Equiaxed growth will occur if,

$$G < 0.617\, N_o^{0.33} \left[1 - \left(\frac{\Delta T_N}{\Delta T_C} \right)^3 \right] \Delta T_C \qquad 4$$

columnar growth will occur if,

$$G > 0.617\, (10 N_o)^{0.33} \left[1 - \left(\frac{\Delta T_N}{\Delta T_C} \right)^3 \right] \Delta T_C \qquad 5$$

where

G= Temperature gradient °C/cm

N_o= Number of nucleation sites per unit volume

ΔT_C= Dendrite tip undercooling °C

ΔT_N= Undercooling for heterogeneous nucleation °C

1.2.6 COMMENTS

Most of the mechanisms presented for the growth of the central equiaxed zone and hence the columnar to equiaxed transition, except the one proposed by Hunt[9] have been based on the generation of nuclei during solidification.

These nuclei are carried to the central region of the casting and form the equiaxed zone. The central region of the casting is at a higher temperature. The main problem is the crystal growth, in which the latent heat generated has to be conducted through liquid above the liquidus temperature which will not occur. The columnar to equiaxed transition is appreciably more complex than suggested by these mechanisms. In addition to the presence of nuclei, a number of other factors must be considered.

i) For a nucleus to grow into an equiaxed grain, the thermal conditions in the melt should be favourable, and at the same time columnar growth has to be supressed.

ii) As dendritic growth proceeds, solute is segregated between dendrites, which strongly influences the liquidus temperature and the freezing rate of the dendrite interface

iii) The composition of the enriched liquid between the dendrites, as a function of distance behind the dendrite tips, may be related to CET.

It is felt that Hunt's model of the CET based on the dendrite tip supercooling, is reasonable, if the measurements of dendrite tip temperatures are accurate. This is because the dendrite tip temperature determines the thermally supercooled region. In addition to this, it is felt that with decreasing growth rates, the supercooling at the dendrite tip decreases rapidly. Accordingly, at low

freezing rates, and little supercooling, the CET should not occur, based on the mechanism proposed by Hunt.

1.3 OBJECTIVES OF THE PRESENT WORK

The primary factors which will be investigated which could contribute to the columnar to equiaxed transition are listed below.

a) The contribution of nucleation generation during soldification to the CET.

b) Thermal conditions during solidification (cooling rate, temperature gradient)

c) Alloy concentration

d) Superheat of the melt.

2. EXPERIMENTAL PROCEDURE

2.1 PREPARATION OF THE ALLOY

Tin-Lead alloys containing 5, 10, and 15wt% lead were used in the investigation of the columnar to equiaxed transition. These alloys were chosen for this investigation because of their low melting points. Depending on the alloy, weighed amounts of 99.9%Sn and 99.9% Pb were melted in a crucible and poured into the mould.

2.2 DETAILS OF THE MOULD

A copper mould was used for solidification. Moulds were made from copper pipe having a wall thickness of 0.32cm. A copper plate was brazed to the bottom of the mould. The height of the mould was 11cm and the internal diameter 3.5cm. The inside of the mould was coated with aquadag to prevent dissolution of copper by the melt. A fibrefrax layer (2mm) thickness was placed adjacent to the copper walls inside and outside the mould. The mould was filled with the required alloy and the alloy rapidly solidified. Then the mould was transferred to the experimental apparatus shown in Fig 9.

2.3 EXPERIMENTAL APPARATUS

This consists of a small resistance furnace surrounding the mould, which remelts the alloy under controlled thermal conditions. The furnace temperature was measured by a

chromel/alumel thermocouple placed inside the furnace and controlled with a temperature controller. The mould, placed in the centre of the furnace rested on a copper block through which water was passed to cool the mould from the bottom.

For the experiments, it was required that heat flow from the mould should be as close to linear as possible along the longitudinal axis of the mould, producing unidirectional solidification. In addition, the rate of solidification and temperature gradient in the melt should be variable.

To obtain unidirectional heat flow, the radial heat losses from the mould have to be balanced by heat from the surrounding furnace. Experiments were carried out initially in which power input to the furnace was varied during solidification to attempt to achieve a balance. This proved to be unsatisfactory. The columnar to equiaxed transition front in these experiments occured in a curved plane with longer columnar grains near the wall as shown in Fig 10. This indicated that the temperature isotherms were not flat which was unsatisfactory. To produce flat isotherms, fibrefrax insulation sleeves were placed against both inside and outside surfaces of the copper tube mould . The insulation effectively stopped radial heat losses and horizontal isotherms were maintained during solidification.

2.4 TEMPERATURE MEASUREMENTS

Temperature measurements in the melt were made at 4 positions, at distances of 2cm, 4cm, 6cm and 8cm from the bottom of the mould. Fig 11 shows schematically the position of the thermocouples in the melt. Chromel/Alumel thermocouples were used. All the thermocouples were calibrated by measuring the freezing temperature of pure tin using an ice-water cold junction. A Kipp and Zonnen chart recorder was used for recording the temperatures. The temperature measurements were accurate within ±0.5°C. Since the temperature at four positions could not be obtained simultaneously, a switching device was used to record the temperature at each position for short intervals. This provided sufficient points to plot the cooling curves. The four thermcouples were inserted in a 0.63cm diameter pyrex tube, which was closed at the bottom. The pyrex tube was inserted in the melt and held vertical with the help of a stand.

2.5 EXPERIMENTAL METHOD

The alloy was melted and was stirred frequently to homogenise the melt. When the melt reached the required temperature, the furnace power was shut off and water passed through the copper chill. This resulted in directional solidification of the melt, progressing from the bottom of the mould. After the metal had solidified and cooled, it was found that the metal could not removed readily from the

mould. As a result the mould was cut with the sample longitudinally. A mould could be used for one experiment only. The sample was polished and etched with a solution containing 1 part nitric acid, 1 part acetic acid and 8 parts glycerol to delineate the cast structure.

2.6 PRINCIPAL VARIABLES

The principal variables believed to influence the columnar to equiaxed transition are

i) Melt composition

i) Melt superheat

iii) Number of nucleation sites in melt

iv) Cooling rate

2.6.1 MELT COMPOSITION

By varying the lead content in the tin-lead alloys, the effect of the melt composition on the CET was studied.

2.6.2 MELT SUPERHEAT

The melt superheat is the temperature difference between the initial temperature of the melt prior to solidification, and the equilibrium liquidus temperature of the alloy. Melt superheat was varied by changing the initial temperature of the melt. The range of superheat examined varied between 10°C to 40°C.

2.6.3 COOLING RATE

The growth velocity and temperature gradient in the melt was varied by changing the heat transfer from the bottom of the mould. This was done by introducing a material of lower thermal conductivity between the mould bottom and the copper chill. This is shown in Fig 12. Stainless Steel was chosen as it has a lower thermal conductivity than copper. The thermal conductivity of copper is 0.93 Cal/sec.cm.°C whereas that of stainless steel is 0.04 Cal/sec.cm.°C. The heat transfer was varied by changing the thickness of the stainless steel.

2.6.4 PRESENCE OF NUCLEATION SITES IN THE MELT

To study the effect of foreign particles acting as heterogenous nucleation sites in the melt, melts were made and cast containing Fe powder. The main reason for choosing Fe powder is that its density (7.87 gms/cm^3) is comparable to the Sn- 10% Pb alloy (7.69 gms/cm^3). In an investigation by Schvezov and Weinberg[36] it was reported that Fe powder could be added to a Sn-Pb melt. The particles were wetted by the melt, did not dissolve significantly, and did not influence the chemisty or temperature distribution in the melt. To establish that Fe powder acted as nucleating sites, two Sn-10%Pb melts were prepared with and without Fe powder. The size of the Fe powder was approximately 5μm in diameter. Both melts were poured into similar graphite moulds and were solidified under identical conditions. The samples, were

then cut, polished, etched, and the microstructure was established as shown in Fig 13. The grain size of the alloy containing Fe powder is 0.3cm, which is smaller than the value of 0.8cm for the alloy without the Fe powder. This shows Fe powder enhances nucleation in the alloy.

2.7 EXPERIMENTS WITH RADIOACTIVE TRACERS

In preliminary experiments, done by earlier workers, radioactive Tl^{204} was added to a Sn-10% Pb alloy which was frozen directionally. The unreported results were used in this investigation to clarify the dendritic structure of the casting and define the primary dendrite arm spacing.

3. HEAT TRANSFER MODEL

Analysis of the temperature gradient at the columnar to equiaxed transition front requires temperature data at points not coincident with the position of the thermocouples. Therefore from the temperature measurements it is difficult to obtain an accurate temperature gradient at any given position in the melt. This difficulty was overcome by developing a heat transfer model of the system and using the four temperature measurements to establish the boundary conditions during solidification.

3.1 OBJECTIVES

The major objectives of the model were to calculate

i) The temperature distribution in the melt at different times during solidification.

ii) The temperature gradient at any desired position.

Fig 14 shows the coordinate system used for the casting. The Z direction is along the cylindrical axis and heat is withdrawn along the Z direction only.

3.2 ASSUMPTIONS

The following assumptions are made in the model.

i) No heat flow from the liquid to the mould occurs in the x,y plane ie. along the radial direction.

ii) Heat is extracted only through the bottom of the mould at Z=HT, as shown in Fig 14. Heat extraction has been characterized using a heat transfer

coefficient which is assumed to be constant.

iii) The thermal conductivity and specific heat of the melt are linearly dependent on temperature.

iv) The melt density is assumed independent of temperature.

v) The latent heat of solidification is released linearly between the liquidus and solidus temperatures. Latent heat is incorporated into the model by increasing the value of the specific heat between the liquidus and solidus temperatures.

$$C_m = C_p + \frac{L}{T_L - T_s} \qquad 6$$

C_m=Effective specific heat

C_p=Normal specific heat

L =Latent heat of solidification

T_L=Liquidus temperaure

T_s=Solidus temperaure

vi) The temperature of the solid-liquid interface is assumed to be equal to the liquidus temperature at all times.

3.3 HEAT FLOW EQUATION

For one dimensional transient heat flow, the heat

transfer equation is

$$K \frac{\partial^2 T}{\partial z^2} = \rho C_p \frac{\partial T}{\partial t} \qquad 7$$

3.4 BOUNDARY CONDITIONS

One initial condition and two boundary conditions are required to solve equation 7.

1) INITIAL CONDITION:

At the beginning of solidification, (t=0) the liquid metal is at a uniform temperature

$$T=T_o \qquad 8$$

2) SURFACE BOUNDARY CONDITION:

i) At time t>0 and at Z=0, there is no heat loss,

$$q=0 \qquad 9$$

ii) At time t>0 and at Z=HT, q is given by

$$q=H(T-T_a) \qquad 10$$

3.5 METHOD OF SOLUTION

The implicit finite difference procedure was used to solve equation 7. The arrangement of the finite difference nodes are shown in Fig 15. The thickness of the nodes perpendicular to the plane of the paper is unity. It is seen from Fig 15, that three different kinds of nodes are present.

i) Top node at I=1

ii) Interior nodes I=2 to N-1

iii) Bottom node I=N

Finite difference equations was obtained performing a heat balance on different nodes. Three equations were derived for the three types of nodes. Details of the finite difference calculations are given in Appendix A. Calculation of the temperature gradient in the melt at a given position is very sensitive to the node size and the time step. Initially a larger time step (2 sec) and node size (1 mm) was used in the finite difference calculations. The results obtained were unsatisfactory. The node size and the time step were decreased to bring stability. Eventually a time step (0.5 sec) and node size (0.5 mm) was used in the calculations. The results obtained were stable. Further decreasing the time step and the node size did not affect the calculation.

3.6 LATENT HEAT RELEASE DURING SOLIDIFICATION

The latent heat is assumed to be released linearly between the liquidus and solidus temperatures . It is essential that the temperature of any node undergoing solidification should fall within the solidus-liquidus range during the calculation. Problems can arise if either the heat extraction is large or the time step involved in the calculation is large. Three types of situations can occur.

i) A node jumps from the liquid to the solid

ii) A node jumps from the liquid to a partial solid

iii) A node jumps from a partial solid to the solid.

To ensure that all nodes fall in the solid/liquid region and

release latent heat, the temperature after each time step was examined and corrected if the node jumped over the solid/liquid region. Three equations for this correction procedure were derived for the three cases described above.

For a node jumping from above the liquidus temperature into the solid/liquid region, (Fig 16) the following equation applies.

The net change in the heat content of a node, due to a drop in temperature from

T_1 to T_2 is$=\rho C_1 V(T_1-T_2)$ 11

If the corrected temperature of the node is T_3, then

$$\rho VC_1(T_1-T_2)=\rho VC_1(T_1-T_L)+\rho VC_2(T_L-T_3) \quad 12$$

$$C_2(T_L-T_3) = C_1(T_L-T_2) \quad 13$$

$$T_3 = T_L - \frac{C_1}{C_2}(T_L-T_2) \quad 14$$

T_3 is the corrected temperature. Similar equations for the other two conditions are given below. If a node jumps from the liquid to the solid, the corrected temperature is:

$$T_3 = T_S -(T_L-T_2)-(T_L-T_S)\frac{C_2}{C_1} \quad 15$$

If a node jumps from the liquid/solid region to the solid: then the corrected temperature is,

$$T_3 = T_S -(T_S-T_2)\frac{C_2}{C_1} \quad 16$$

3.7 INPUT PARAMETERS

The various input parameters used in the model are listed below for the Sn-10% Pb alloy.

Solidus temperature	183°C
Liquidus temperature	215°C
Latent heat of solidification	13.5 cal/gm
Density	7.7 gm/cc
Specific heat	0.06 cal/gm°C
Thermal conductivity	(-0.0000864xTemp+0.15194) Cal/cm°C
Node size	0.05cm
Time step	0.5sec
Length of casting	10cm

3.8 CALCULATION OF HEAT TRANSFER COEFFICIENT

To calculate the temperature distribution in the alloy during solidification, a value for the heat transfer coefficient at the bottom and top of the mould was assumed. The temperature distribution in the melt was calculated as a function of the position and time of solidification. These values were then compared to the experimental temperature measurements made at four points in the melt. The heat transfer coefficient was then modified and the temperature distribution in the melt recalculated. This process was repeated until the calculated temperatures were in agreement with the measured temperatures to within ±3.0°C.

After establishing the heat transfer coefficient, the model was used to calculate the temperature gradient in the melt as a function of the position and time.

The measured and computed temperatures for one experiment is plotted in Fig 17.

4. RESULTS

The temperature measurements made during solidification were used in the heat transfer model to establish the heat transfer coefficient at the bottom of the mould.

4.1 RESULTS FOR THE SN-10%PB ALLOY

The Sn-10%Pb alloy was chosen as the initial alloy in this investigation. After completion of each experiment, the samples were sectioned longitudinally, polished, etched and the macrostructure establshed. If the columnar to equiaxed transition had occured, the position of transition was measured and the length of the columnar zone determined.

Table I summarises the results obtained for the Sn-10%Pb alloy. It gives the initial temperature of the melt, the superheat, the position of transition and the heat transfer coefficient used. Photographs of the structure of typical samples are shown in Fig 18. A columnar structure is observed starting at the bottom of the sample with the grain boundaries and the primary dendrite axes parallel to the growth direction. The columnar to equiaxed transition is observed to be sharp and quite flat. The equiaxed grains are prominent, have random orientations, and tend to decrease in diameter with increasing distance above the transition plane.

4.1.1 EFFECT OF COOLING RATE ON COLUMNAR ZONE LENGTH

The columnar zone length, measured from the bottom of the sample, is plotted in Fig 19 as a function of the heat transfer coefficient. It is seen that the columnar zone length varies linearly with the heat transfer coefficient in the range examined. Since the cooling rate is proportional to the heat transfer coefficient, the columnar zone length is proportional to the cooling rate. The columnar zone length therefore increases with an increase in the cooling rate. Fig 20 is a plot of the percentage of the equiaxed grains as a function of the heat transfer coefficient. The percentage of the equiaxed grains is observed to decrease with increasing values of the heat transfer coefficient.

The observed dependence of the columnar zone length on the cooling rate suggests that the CET is related to the temperature gradient at the advancing columnar front. The transition may occur at a critical temperature gradient.

4.1.2 MEASUREMENT OF TEMPERATURE GRADIENT

By using different values of the heat transfer coefficient in the heat transfer model, the temperature gradient in the melt can be calculated as a function of position and time during solidification for different freezing rates.

The temperature gradient in the melt at increasing distances from the chill face for the twelve tests are listed in Table II. The temperature gradient at the position

at which the CET occured is listed in the final column of the Table. It is seen that the transition temperature gradient is between 0.99 to 1.06°C/cm.

In some tests, the columnar to equiaxed transition did not occur. Photographs of two samples without any transition are shown in Fig 21 in which the columnar grains extend to the top of the sample. Calculations of the temperature gradient for these samples were made, giving the values listed in Table III. The temperature gradient in the samples which did not exhibit CET are shown to be higher than 1.06°C/cm. From these results it appears that a necessary condition for the columnar to equiaxed transition to occur in Sn-10%Pb is that the temperature gradient at the advancing columnar interface must be at, or below, 1.06°C/cm. Averaging the results gives a critical temperature gradient for the columnar to equiaxed transition in Sn-10%Pb alloy as 1.02°C/cm.

The temperature gradient in the melt as a function of the distance from the chilled end is plotted in Fig 22 for a series of heat transfer coefficients. The temperature gradient is observed to decrease with increasing distances from the chill end. The horizontal line indicates the critical temperature gradient at which columnar to equiaxed transition occurs. The position at which the horizontal line intersects the curves for test 1, test 3 and test 6, indicates where the CET should occur. The experimentally determined positions of the CET for different tests are

marked by the vertical lines. For test 14 and test 15, the minimum temperature gradient in the melt is 1.15 and 1.20°C/cm respectively. This is higher than the critical temperature gradient for the CET as indicated by the horizontal line. Therefore the CET is not expected to occur.

4.1.3 EFFECT OF SUPERHEAT

The effect of the melt superheat on the CET was studied. The columnar zone lengths measured for different melt superheats and different heat transfer coefficients are listed in Table IV. The columnar zone length is observed to remain essentially constant for different melt superheats for the same heat transfer coefficient. This is shown more clearly in Fig 23 where the columnar zone length has been plotted as a function of the melt superheat for the four heat transfer coefficients examined. The essentially horizontal curves show that the columnar zone length is independent of the melt superheat for the same cooling rate. Photographs of three etched samples, cast with different superheats, with the same cooling rate are shown in Fig 24. The columnar zone length in the three samples is observed to be similar. The temperature distribution in the melt during solidification as a function of time is shown in Fig 25. In the beginning the temperature profile is steep. With time the temperature profile reaches a steady state as shown in Fig 25. This is because, the heat transfer in the melt occurs by conduction which is mainly controlled by the

thermal conductivity of the melt. The thermal conductivity is constant in the range of temperature examined. Therefore the temperature distribution in the melt reaches a steady state. For melts with different superheats, steady state is reached at different times. This is shown more clearly in Fig26.

4.1.4 EFFECT OF NUCLEATING SITES

The presence or generation of nuclei in the melt is considered in the literature to be of major significance in the columnar to equiaxed transition. In particular attention is directed to the production of nuclei in the melt leading to the formation of equiaxed grains. Few experiments are reported in which nuclei were introduced in the melt, in the form of foreign particles, to reduce the necessity to produce nuclei during solidification. Two directional castings were made with Fe powder added to the melt. The results obtained are listed in Table V. The appearance of the etched sample treated with Fe powder is shown in Fig 27. In test 5, table V, the CET occured at a temperature gradient of 1.03°C/cm, which is similar to that observed in experiments where no Fe powder was added. In test 14, table V the temperature gradient in the melt did not reach the critical temperature gradient, and no CET was observed. These results clearly indicate that the columnar to equiaxed transition is not dependent on the number of nucleation sites in the melt or, therefore, on the generation of nuclei

during solidification.

4.2 EFFECT OF SOLUTE CONTENT

It was expected that the composition of the alloy would also influence the CET, since pure metals do not exhibit a CET in directional solidification. Experiments were conducted on alloys of Sn containing 5 and 15wt% Pb using the standard experimental procedure. The position of the CET for the Sn-15wt%Pb alloys are listed in Table V and the corresponding temperature and temperature gradient distribution in Table VII. The final column in Table VII indicates that the columnar to equiaxed transition occurs at a temperature gradient in the range of 1.23-1.28°C/cm which is higher than that of Sn-10%Pb alloy. The corresponding results from Sn-5%Pb alloy are listed in Tables VIII and Table IX. The temperature gradients listed in Table IX show that the gradients at the columnar to equiaxed transition are in the range of 0.90-0.94°C/cm. This is lower than that observed for the Sn-10%Pb alloy.

The temperature gradients in the melt, as a function of the distance from the chill end for Sn-15%Pb and Sn-5%Pb are plotted in Fig 28 and 29 respectively The horizontal lines in the figures indicate the critical temperature gradient for the columnar to equiaxed transition.

The columnar zone length as a function of the heat transfer coefficient for Sn-15%Pb and Sn-5%Pb is shown in Fig 30 and 31 There is a linear dependence of the columnar

zone length on the heat transfer coefficient over the range examined. To get a better indication of the effect of the solute content on the columnar zone length, for the different alloys studied, the columnar zone length has been plotted as a function of the heat transfer coefficient for the three alloys in Fig 32. The increase in Pb content of the alloy decreases the columnar zone length for the same heat transfer coefficient. This is shown more clearly in Fig 33 where the columnar zone length is plotted as a function of Wt % Pb for three heat transfer coefficients.

The critical temperature gradient observed for the CET in the three alloys examined is listed in Table X. The critical temperature gradient in the melt as a function of Pb content is shown in Fig 34. It shows that with an increase in Pb content in the alloy, the critical temperature gradient for the CET is increased. Therefore, with higher lead concentrations, the transition occurs closer to the chill end.

5. DISCUSSION

From the experimental results, two factors appear to control the columnar to equiaxed transition. They are

i) The temperature distribution in the melt. The transition occurs when a specific low temperature gradient is reached at the leading edge of the solid/liquid interface. The critical temperature gradient is a function of the alloy solute content.

ii) Increasing the Pb content in the Sn-Pb alloy shifts the CET to a position closer to the chill end, decreasing the columnar zone length.

The mechanism of the columnar to equiaxed transition can be divided into two parts.

i) The presence or formation of nuclei in the melt.

ii) The growth of these nuclei into equiaxed grains, supressing columnar growth.

Most of the theories in the literature have focussed on the formation of nuclei in the melt,the nuclei eventually growing and forming the central equiaxed zone.

In the present experiments directional solidification was vertically upwards. In this case, the temperature in the melt increases from the bottom to the top of the mould. This results in little or no convection in the liquid due to buoyancy forces. Convection is a basic component in the generation of nuclei by crystal multiplication. Therefore it is considered that in the present experiments nuclei cannot be generated by the multiplication mechanisms proposed.

Further, additions of Fe powder which acted as nucleants did not change the position of CET. These observations therefore suggest that the central equiaxed zone forms from nuclei already present in the melt.

Assuming that many nuclei are present in the melt, the formation of equiaxed grains, will depend on the local thermal conditions which allow the nuclei to grow. The possibility that consitutional supercooling is present in the melt, ahead of the solid-liquid interface, has been examined. When an alloy of composition C_o, as shown in Fig 35 solidifies and if the solid/liquid interface is flat, the concentration profile in the liquid ahead of the solid/liquid interface with no mixing in the liquid is of the form shown in Fig 36. There is a solute build up ahead of the interface which results in constitutional supercooling of the liquid metal ahead of the interface, in the presence of a shallow temperature gradient. Usually solidification occurs dendritically. In the case of dendritic solidification, solute segregation occurs primarily between the dendrites, giving the solute distribution in the liquid ahead of the columnar interface shown in Fig 37. There is no solute enrichment of the liquid ahead of the interface. Therefore constitutional supercooling of the melt ahead of the columnar dendritic front is not likely to occur. From the experimental results, the temperature gradient at the transition, although small, is not zero. This means that, ahead of the columnar

interface, the temperature of the melt is higher than the equilibrium liquidus temperature of the alloy. Hence equiaxed grains do not grow.

The liquid concentration in the interdendritic region between columnar dendrites has been considered to determine if conditions are favourable for the growth of equiaxed grains.

A simple analytical expression has been derived to calculate the liquid composition between dendrites.

Two primary dendrites are represented by two flat parallel plates, with the interdendritic spacing L as shown in Fig 38. Solidification occurs by thickening of these plates in the x direction with a freezing rate of R. Solute is rejected during solidification into the interdendritic liquid. The interdendritic liquid composition has been calculated assuming the following,

a) No diffusion occurs in the solid.

b) There is no liquid mixing in the interdendritic region. Solute transport is by diffusion only.

c) Equilibrium is assumed at the solid/liquid interface. Thus the liquid composition at the interface is known from the phase diagram.

d) The rate of change of concentration of liquid with time is independent of position.[37]

From Fick's second law

$$\frac{\partial^2 C_L}{\partial x^2} = \frac{1}{D} \frac{\partial C_L}{\partial t} \qquad 17$$

The boundary conditions are (Fig 39)

$$\text{at } x = 0 \quad C_L = C_m \qquad 18$$

$$\text{at } x = a \quad C_L = C_i \qquad 19$$

$$\text{at } x = 0 \quad \frac{\partial C_L}{\partial x} = 0 \qquad 20$$

Integrating equation 17 gives

$$\frac{\partial C_L}{\partial x} = \frac{1}{D} \frac{\partial C_L}{\partial t} x + A_1 \qquad 21$$

where A_1 is a constant.

Substituting the boundary condition $x=0$, $\frac{\partial C_L}{\partial x} = 0$ in equation 21 gives $A_1=0$

$$\frac{\partial C_L}{\partial x} = \frac{1}{D} \frac{\partial C_L}{\partial t} x \qquad 22$$

Integrating equation 22 gives

$$C_L = \frac{x^2}{2D} \frac{\partial C_L}{\partial t} + A_2 \qquad 23$$

where A_2 is a constant

Substituting the boundary condition $x=0$, $C=C_m$ in equation 23

gives

$$A_2 = C_m$$

$$C_L = \frac{x^2}{2D} \frac{\partial C_L}{\partial t} + C_m$$

$$C_L - C_m = \frac{x^2}{2D} \frac{\partial C_L}{\partial t} \qquad 24$$

To know the liquid composition from equation 24, value of $\frac{\partial C_L}{\partial t}$ must be known.

A quantitative solute mass balance has been obtained by equating the amount of solute rejected from the solid/liquid interface to the increase in solute of the remaining liquid. From Fig 40

$$(C_L - C_s)df_s = f_L \, dC_L \qquad 25$$

$$f_s + f_L = 1$$

$$df_s = -df_L \qquad 26$$

$$C_s = kC_L \qquad 27$$

substituting equations 26 and 27 in 25 gives

$$-C_L\,(1-k)\,df_L = f_L\,dC_L \qquad 28$$

$$\frac{df_L}{f_L} = -\frac{dC_L}{C_L\,(1-k)}$$

Integrating equation 28 from $C_L=C_o$ at $f_L=1$ gives

$$C_L = C_o f_L^{k-1} \qquad 29$$

Differentiating equation 29 with time gives

$$\frac{\partial C_L}{\partial t} = \frac{C_o(1-k)}{f_L^{2-k}}\,\frac{df_L}{dt} \qquad 30$$

From Fig 38, fraction solid f_s is given by,

$$f_s = 1 - \frac{2x}{L} \qquad 31$$

Differentiating equation 31 with time gives

$$\frac{df_s}{dt} = -2\frac{dx}{dt}\,\frac{1}{L}$$

Where $\frac{dx}{dt}$ = lateral growth velocity of dendrite 'R'

$$\frac{df_s}{dt} = -\frac{2R}{L} \qquad 32$$

$$f_s = 1 - f_L$$

$$\frac{df_s}{dt} = -\frac{df_L}{dt} \qquad 33$$

Substituting $\frac{df_s}{dt}$ in equation 32

$$\frac{df_L}{dt} = \frac{2R}{L} \qquad 34$$

Substituting $\frac{df_L}{dt}$ in equation 30 gives

$$\frac{\partial C_L}{\partial t} = \frac{C_o(1-k)}{f_L^{2-k}} \frac{2R}{L} \qquad 35$$

Substituting $\frac{\partial C_L}{\partial t}$ in equation 24 gives,

$$C_L - C_m = \frac{x^2}{2D} \frac{C_o(1-k)}{f_L^{2-k}} \frac{2R}{L} \qquad 36$$

In the initial stages of solidification $f_L=1$, thus

$$C_L - C_m = \frac{x^2}{2D} C_o(1-k) \frac{2R}{L} \qquad 37$$

The interdendritic liquid composition can be calculated from equation 37 knowing the dendrite spacing L, freezing rate R, diffusion coefficient D and the partition coefficient k. The interdendritic spacing L was obtained from the sample which contained radioactive tracer Tl^{204}. The autoradiograph is shown in Fig 41. A value for freezing rate R was assumed for the calculation. The following values are used in the calculation

$L = 3.33 \times 10^{-2}$cm

$R = 8 \times 10^{-4}$cm/sec

$D = 5 \times 10^{-5}$cm^2/sec

$k = 0.0877$

$C_o = 10\%Pb$

The composition of the liquid along a given line A_1A_2 in the interdendritic region (Fig 42) was calculated using eq 37. The liquid composition at the solid/liquid interface A_1A_2 is obtained from the phase diagram knowing the temperature of the liquid. The temperature of liquid between A_1 and A_2 is taken as constant since the isotherms are planar. The results are listed in Table X and are shown in Fig 43. The equilibrium liquidus temperature along A_1A_2 corresponding to the composition, variation is shown in Fig 44. The actual temperature of the liquid is also shown. From Fig 44 the liquid along A_1 A_2 is observed to be constitutionally supercooled. At the centre of the interdendritic region, the supercooling a is maximum. For Sn-10%Pb, the maximum supercooling that is obtained is 1.40°C.

5.1 MECHANISM FOR THE COLUMNAR TO EQUIAXED TRANSITION

The liquid in the interdendritic region is shown to be constitutionally supercooled,which would allow nuclei to grow into equiaxed grains. From the experimental results, it has been shown that the temperature gradient in the melt and the solute content of the alloy influence the columnar to equiaxed transition. In some experiments, when the cooling rate was high, the CET could not be obtained. This indicates that a steep temperature gradient in the melt enhances columnar growth.

It is considered that the columnar to equiaxed transition is determined by the competitive growth of the columnar grains and the equiaxed grains. Fig 45 shows a schematic section of a columnar dendrite A and a nucleus B in the interdendritic region. The liquid surrounding the columnar dendrite is richer in solute than the liquid surrounding nucleus B. Therefore the liquid surrounding the columnar dendrite has a lower freezing temperature than the liquid surrounding the nuclei. Enriched liquid hinders the growth of columnar dendrites because of the lower freezing temperature. However, when the temperature gradient in the melt is high, as is the case with higher cooling rates, columnar growth is favoured. As the temperature gradient in the melt is reduced, thermal conditions are not favourable for the growth of a columnar dendrite. In addition to this, columnar growth is further hindered due to the enriched liquid adjacent to it. Nuclei available in the interdendritic liquid can grow, and form equiaxed grains because of the supercooling available. Once equiaxed grains start growing, the growth of columnar grain is stopped thus resulting in a columnar to equiaxed transition. A higher temperature gradient in the melt and a lower solute content favour columnar growth. A lower temperature gradient and higher solute content favour equiaxed growth. For different Pb contents, in Sn-Pb alloys, the maximum supercooling that is obtained in the interdendritic region is listed in Table XI. The supercooling is increased with an increase in

the Pb content. Therefore the central equiaxed zone is greater in a casting of Sn-15%Pb as compared to a casting of Sn-5%Pb alloy.

6. CONCLUSIONS

The columnar to equiaxed transition occurs when a critical temperature gradient is reached at the leading edge of the solid/liquid interface. The critical temperature gradient is small but not equal to zero. The critical temperature gradient is increases with an increase in the solute content of the alloy. The length of the columnar zone in a casting can be predicted, if the cooling conditions are known. An increase in solute content of the alloy increases the size of the equiaxed zone. This is because the constitutional supercooling in the interdendritic region is increased with an increase in solute content of the alloy. The columnar zone length is increased with an increase in the heat extraction rate, for the three alloys examined. It is also seen that for a given alloy, superheat of the melt does not affect the columnar zone length, if the cooling rate is the same. In the type of experiments conducted it is seen that the columnar to equiaxed transition is not controlled by the generation of nuclei in the melt during solidification. Finally, the structure of a casting is determined by competitive growth between the growing columnar grains and the equiaxed grains. A higher temperature gradient in the melt favour growth of columnar grains and thus equiaxed grains cannot compete. However as the temperature gradient decreases, columnar grain growth is supressed. Equiaxed grains can nucleate and grow because of the supercooling available in the interdendritic liquid.

Columnar grains cannot compete, resulting in a columnar to equiaxed transition.

BIBLIOGRAPHY

1. B.Chalmers: Principles of Solidification, 1964, Wiley, N.Y.

2. D.Walton,B.Chalmers: TMS-AIME, 1959 Vol.215, p.447

3. G.S.Cole: Structure of Ingot casting, Course on Solidification, Grenoble, France

4. M.Prates and H.Biloni: Met. Trans., Vol.13, 1972 p.1501

5. F.T.Bomer, C.M.Fleming: TMS-AIME, Vol.239, 1967 p.218

6. F.R.Herzel: TMS-AIME, Vol.124, 1937 p300

7. J.Lipton, W.Kurz and W.Heinemann: Arch. Eisenhuttenwes, Vol.55, 1984, p195

8. R.Gender: Journal Inst. of Metal, Vol.35, 1926, p259

9. J.K.Brimacombe and K.Sorimachi: Met. Trans., Vol.8B, 1977, p489

10. W.C.Winegard, B.Chalmers: Trans. Am. Soc. Metals, Vol.46, 1954, p.1214

11. B.Chalmers: Aust. Inst. Metals, Vol.8, Aug 1963, p.225

12. K.A. Jackson, J.D.Hunt, D.R.Uhlmann and T.P.Seward: TMS-AIME, Vol.236, Feb 1966, p.149

13. R.T.Southin: TMS-AIME, Vol.230, Feb 1967, p.220

14. N.Biloni, B.Chalmers: Journal of Materials Science, Vol.3, 1948, p.139

15. R.Morando, H.Biloni, G.S.Cole and G.F.Bolling: Met. Trans., Vol.11, 1970, p1407

16. S.E.KisaKusck: Journal of Material Science, Vol.19, 1984, p.2289

17. A.Ohno and H.Soda: Trans. ISIJ, Vol.10, 1970, p.13

18. R.D.Doherty,P.D.Cooper, M.H.Bradbury and F.J.Honey: Met. Trans., Vol.8A, 1977, p.397

19. J.D.Hunt: Materials Science & Eng., Vol.65, 1984, p.75

20. S.C.Flood and J.D.Hunt: Modelling of casting and welding processes, 1980, p.207

21. M.H.Burden and J.D.Hunt: Met. Trans., Vol.6A, 1975,

p.240

22. J.W.Rutters and B.Chalmers: Can. J. Physics, Vol.31, 1953, p.15

23. W.A.Tillers and J.W.Rutters: Can. J. Physics, Vol.32, 1956, p.96

24. G.S.Cole and G.F.Bolling: TMS-AIME, Vol.242, 1968, p.153

25. R.J.Schafer and M.E.Glicksman: TMS-AIME, Vol.239, 1967, p.257

26. G.S.Cole and G.F.Bolling: TMS-AIME, Vol.233, 1965, p.233

27. G.S.Cole and G.F.Bolling: TMS-AIME, Vol.236, 1966, p.1366

28. G.S.Cole and G.F.Bolling: TMS-AIME, Vol.239, 1967, p.1824

29. F.C.Langenberg, G.Pestel and C.R.Honeycutt: TMS-AIME, Vol.221, 1961, p.993

30. F.A.Crossley, R.D.Fisher and A.G.Metcalfe: TMS-AIME, Vol.221, 1961, p.419

31. A.A.Tzavaras: Steel Making Proceedings, Vol.66, 1983, p.89

32. G.S.Cole and G.F.Bolling: TMS-AIME, Vol.239, 1967, p.1824

33. D.R.Uhlmann, T.P.Seward and B.Chalmers et al: TMS-AIME, Vol.236, 1966, p.527

34. M.H.Burden and J.D.Hunt: Journal of Crystal Growth, Vol.22, 1974, p.99

35. M.H.Burden and J.D.Hunt: Journal of Crystal Growth, Vol.22, 1974, p.109

36. C.Schvezov and F.Weinberg: M.A.Sc. Thesis, 1983, Interaction of particle with an advancing solid/liquid interface, Univ. of B.C.

37. P.K.Rohatagi and Clyde M. Adams Jr.: TMS-AIME, Vol.239, 1967, p.1737

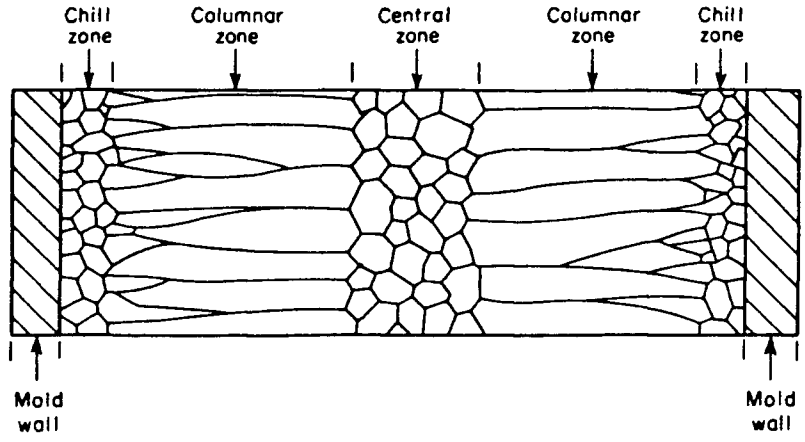

Figure 1 - Macrostructure of a casting showing the three different zones

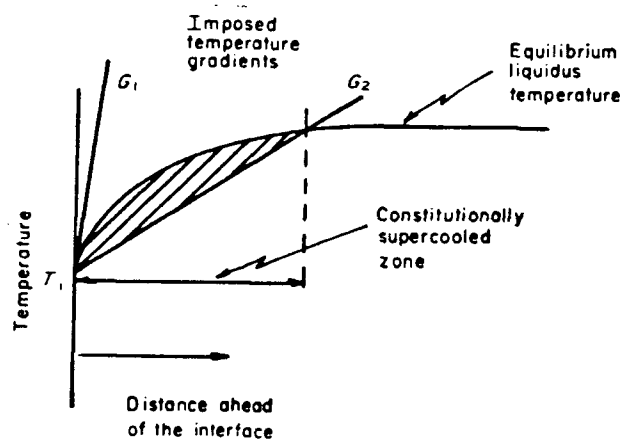

Figure 2 - Constitutional supercooling ahead of an interface

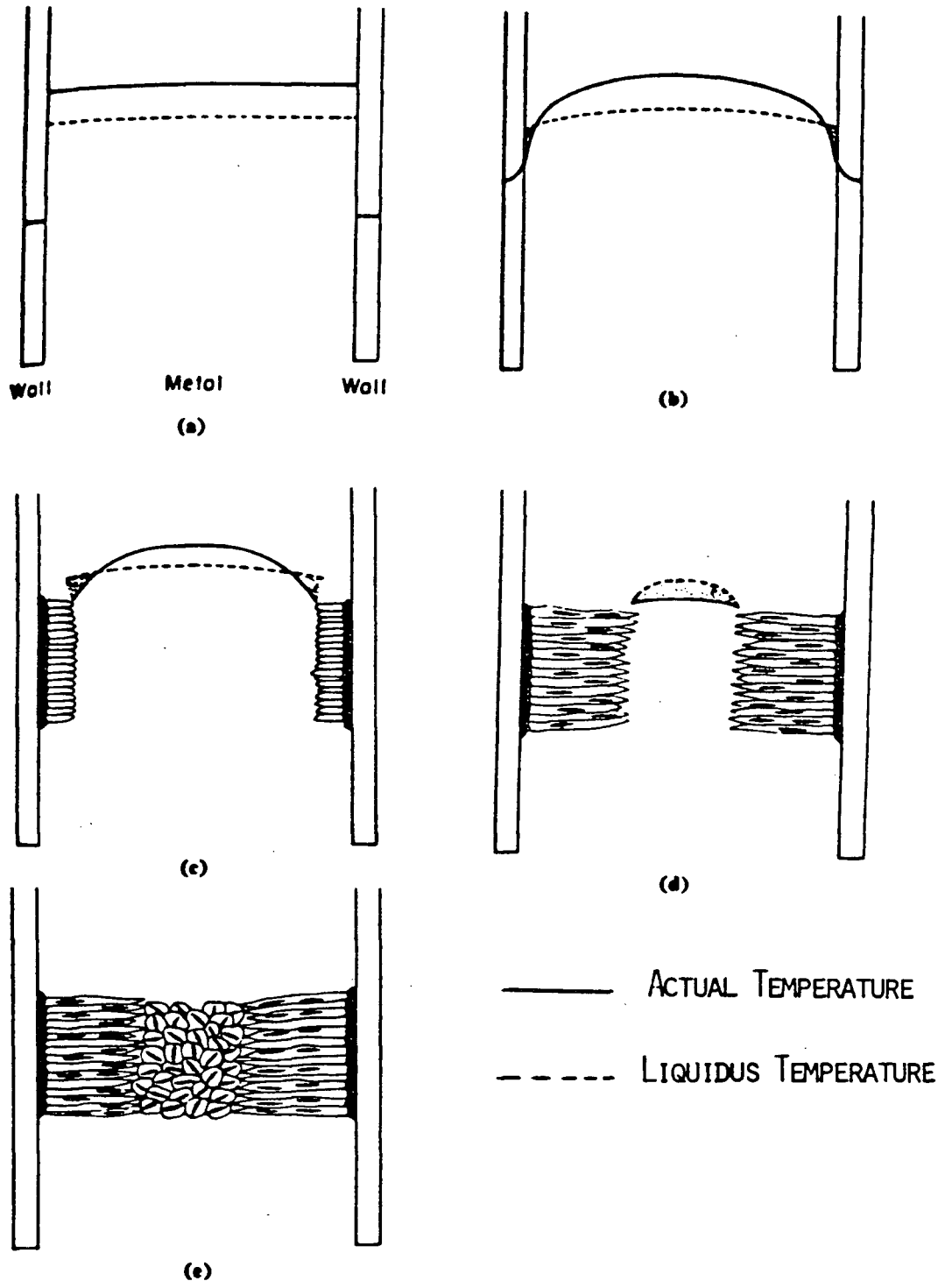

Figure 3 - (a-e) Sequence of events leading to the formation of equiaxed zone based on the concept of constitutional supercooling

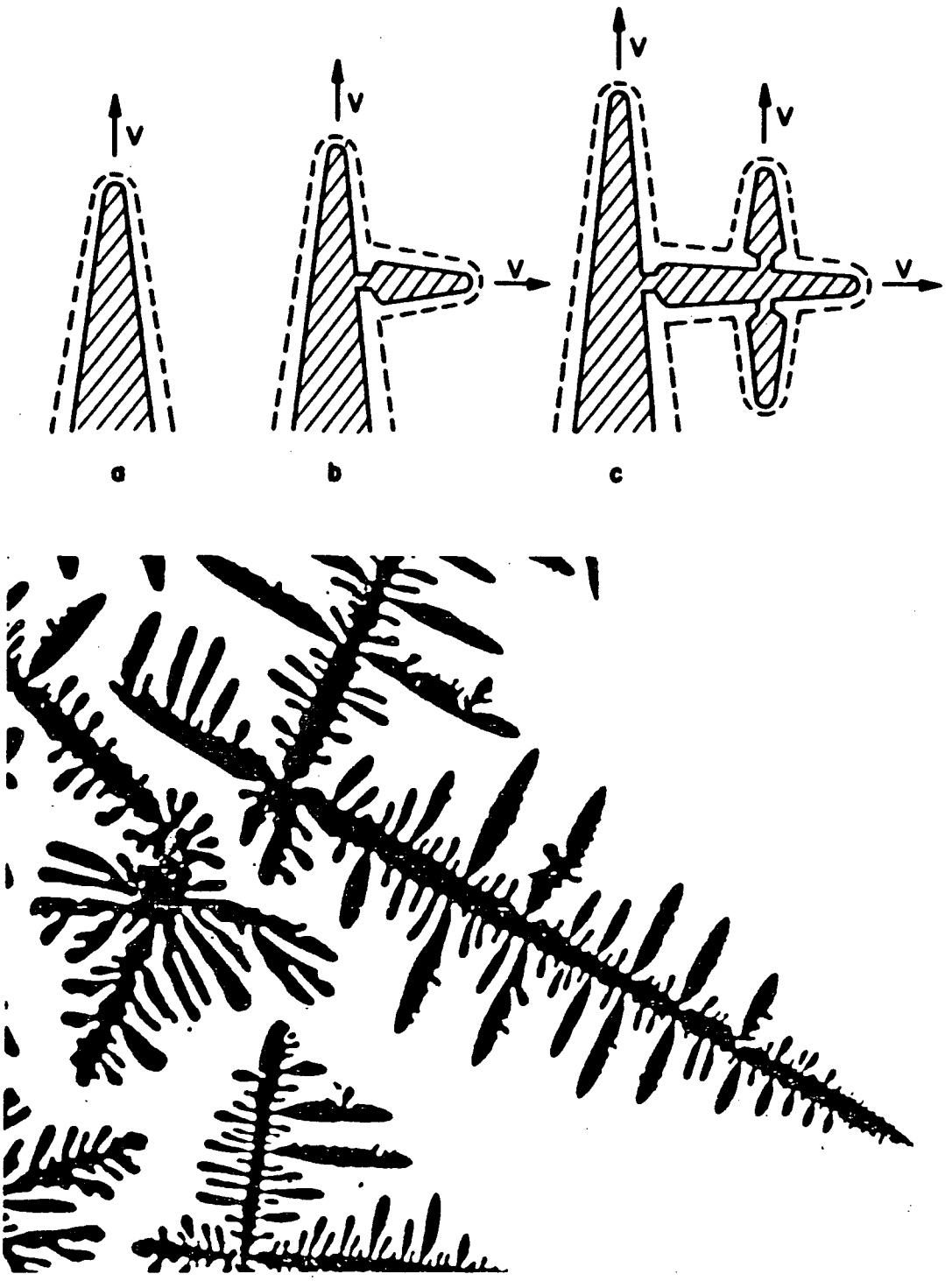

Figure 4 - Necking at the junction between the primary and the secondary dendrite and the secondary and the tertiary dendrite

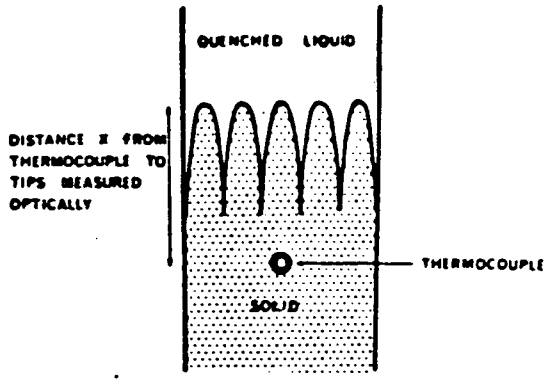

(a)

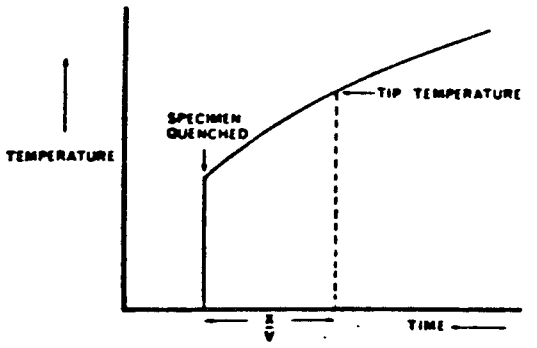

(b)

Figure 5 - a) Specimen grown at a constant velocity V and quenched, b) A temperature/time trace of the thermocouple in the specimen

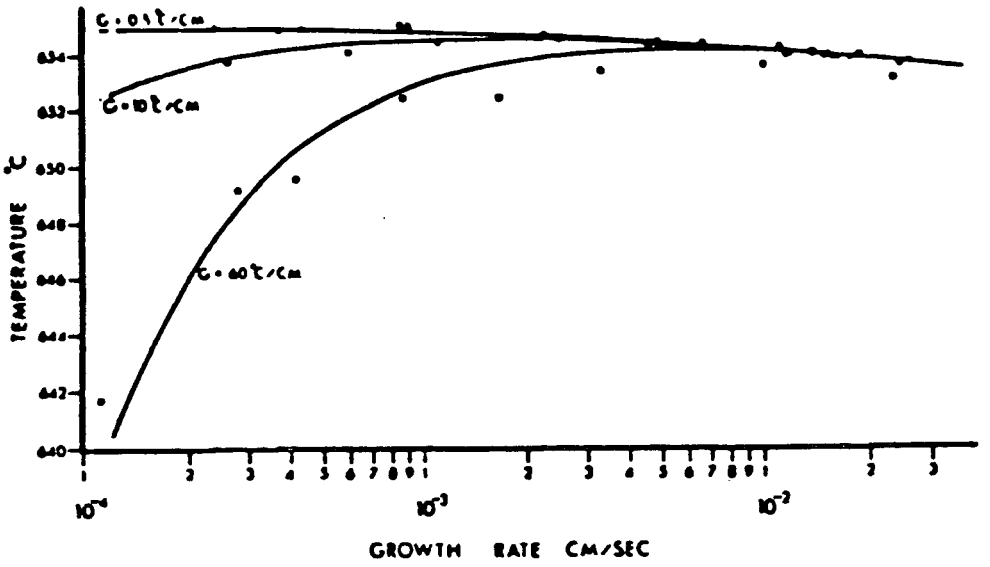

Figure 6 - Variation of the dendrite tip temperature of Al-2%wtCu with the growth velocity at temperature gradients of 0.5,.10 and 60 °C/cm

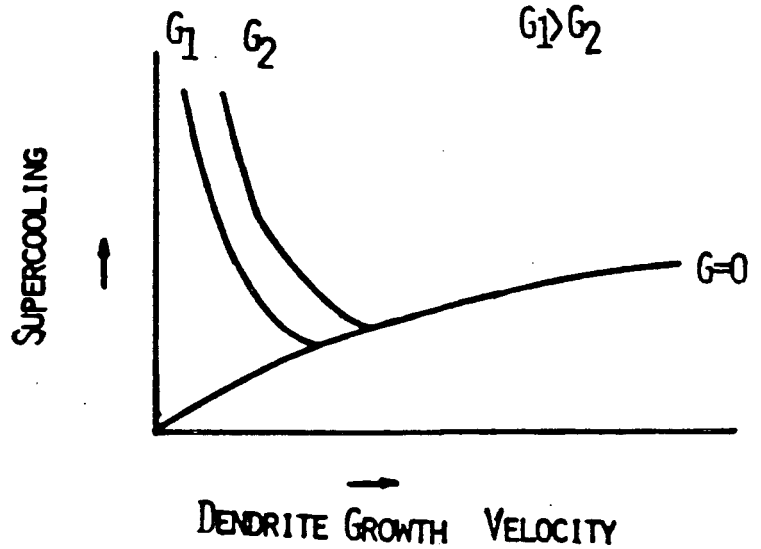

Figure 7 - Variation of the dendrite tip supercooling with dendrite growth velocity for three different temperature gradients, G in the liquid ahead of the growing columnar dendrites

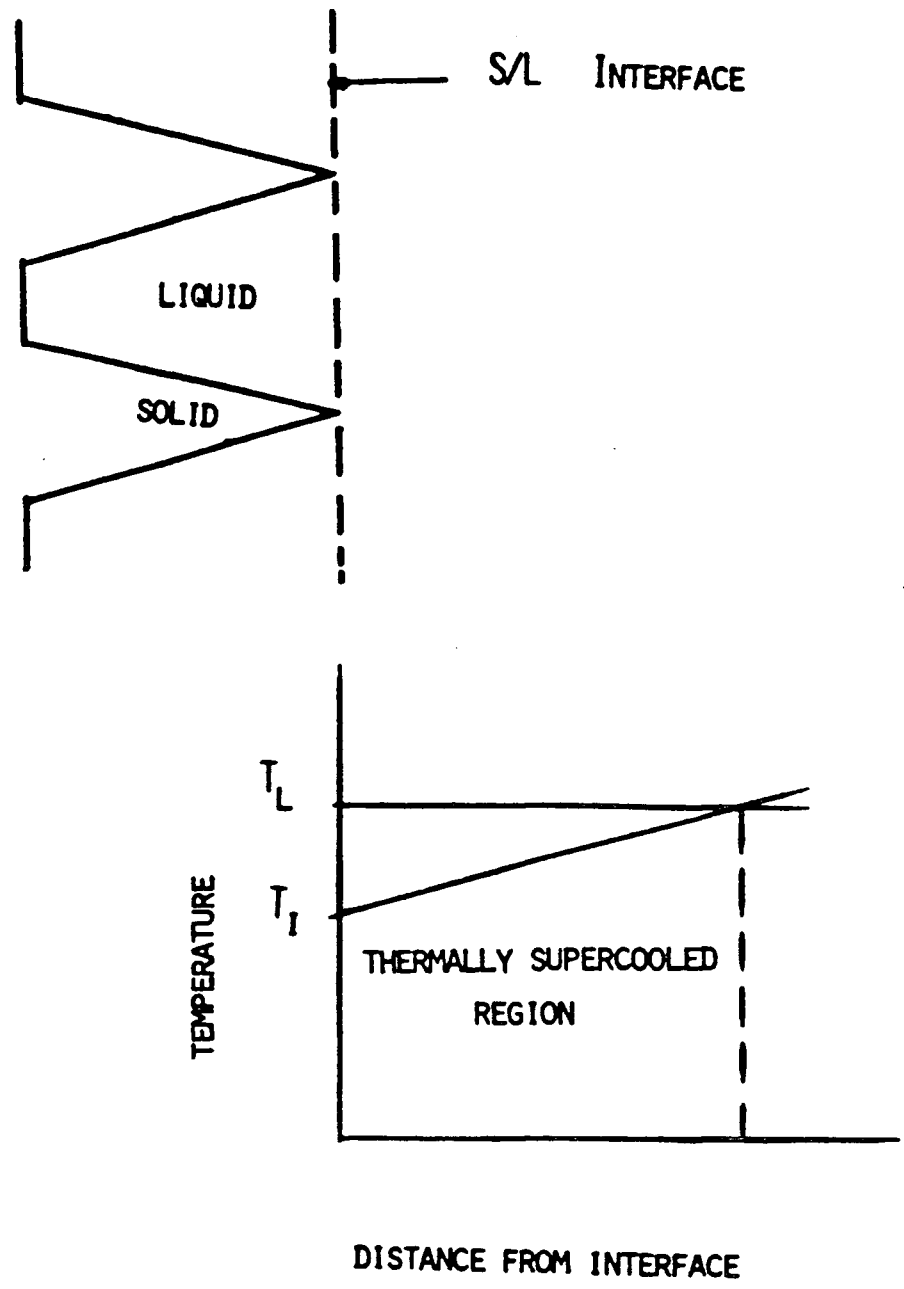

Figure 8 - Thermal supercooling of the liquid ahead of the growing columnar dendrites

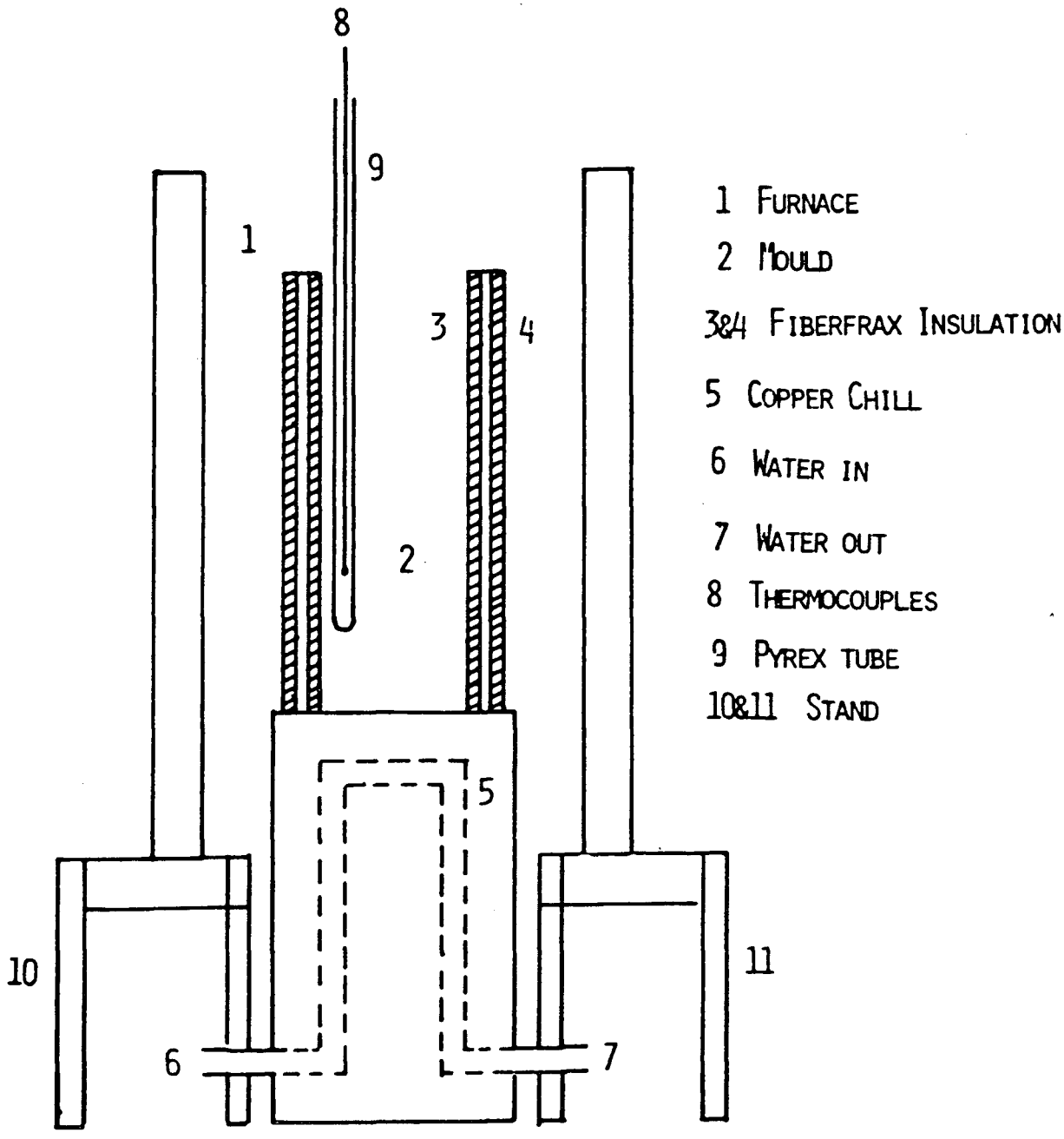

Figure 9 - Schematic illustration of the apparatus for directional solidification.

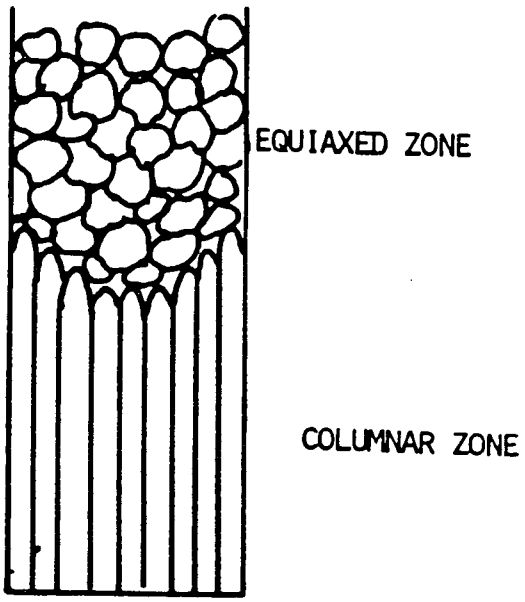

Figure 10 - Longer columnar dendrites at the side of the casting than at the centre due to the heat losses from the mould wall.

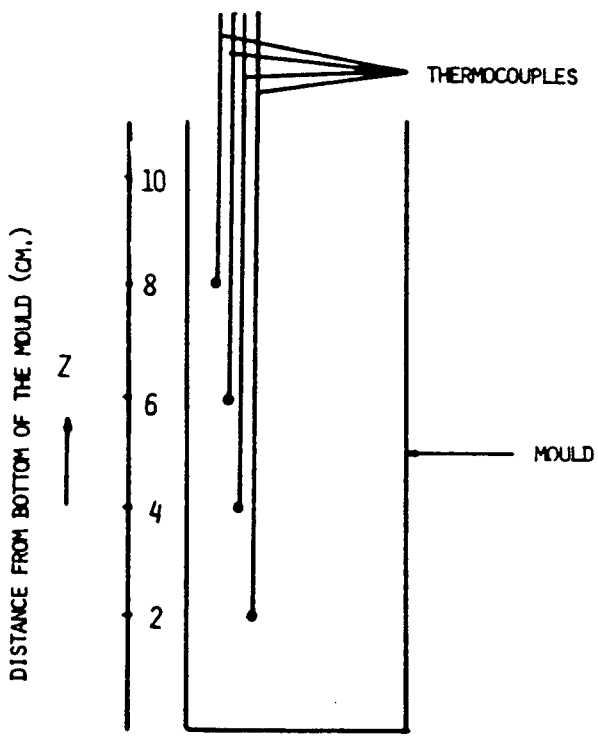

Figure 11 - Position of the four thermocouples in the melt during solidification.

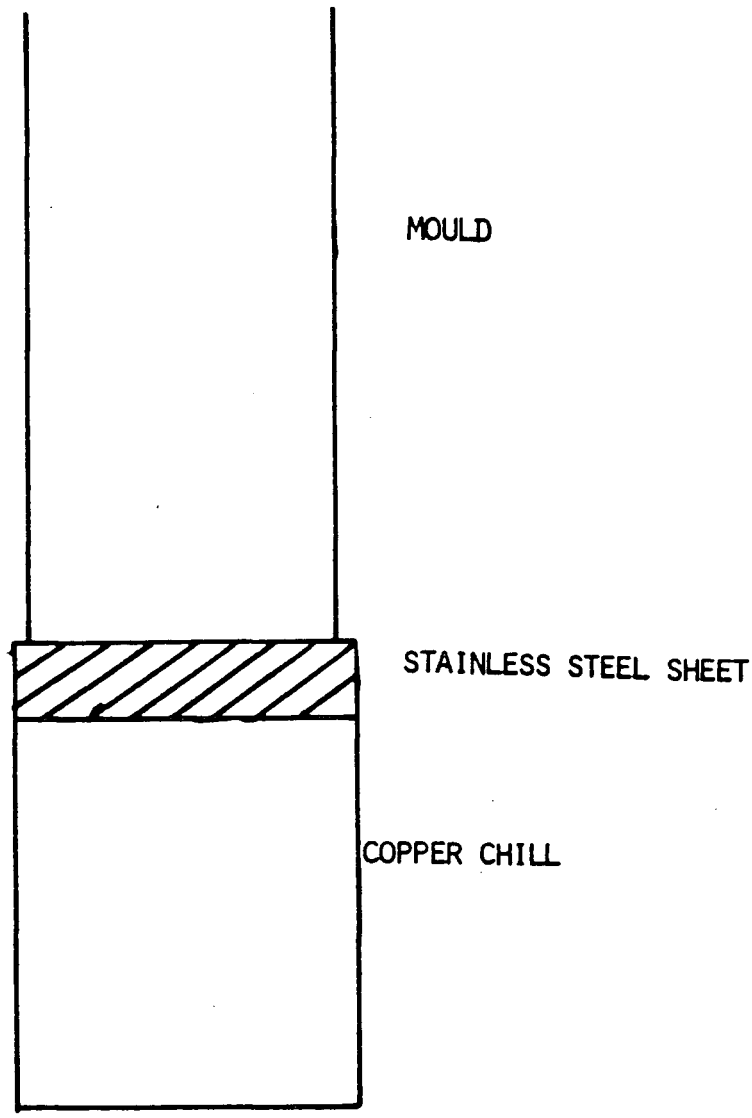

Figure 12 - Introduction of the stainless steel sheet between the bottom of the mould and copper chill to reduce heat transfer.

a

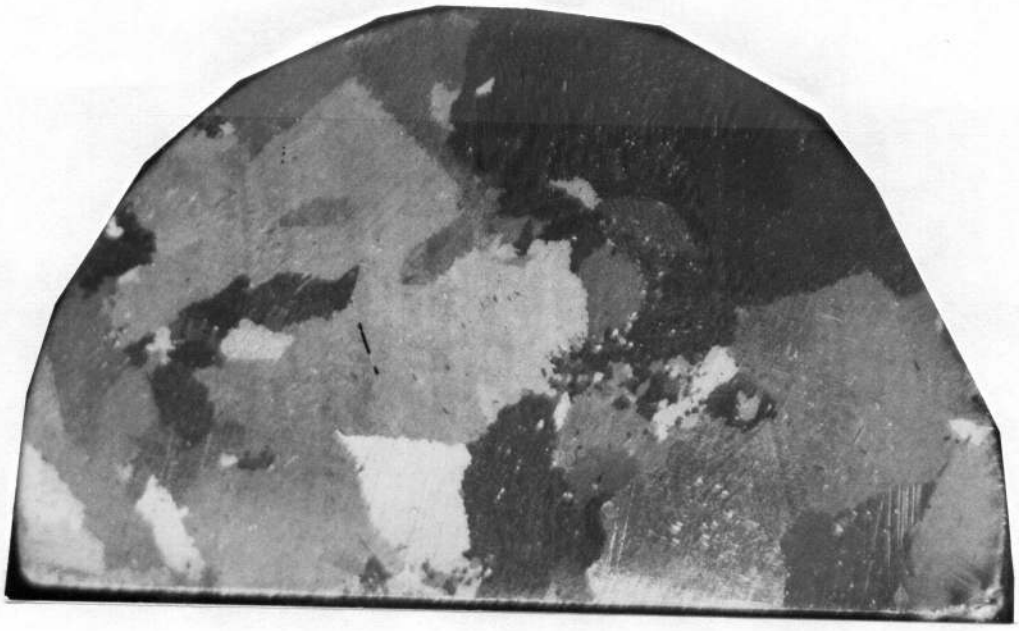

b

Figure 13 - Structure of a casting a) with the addition of Fe powder to the melt showing fine grains. b) without the addition of Fe powder, showing coarse grains. Mag 4X.

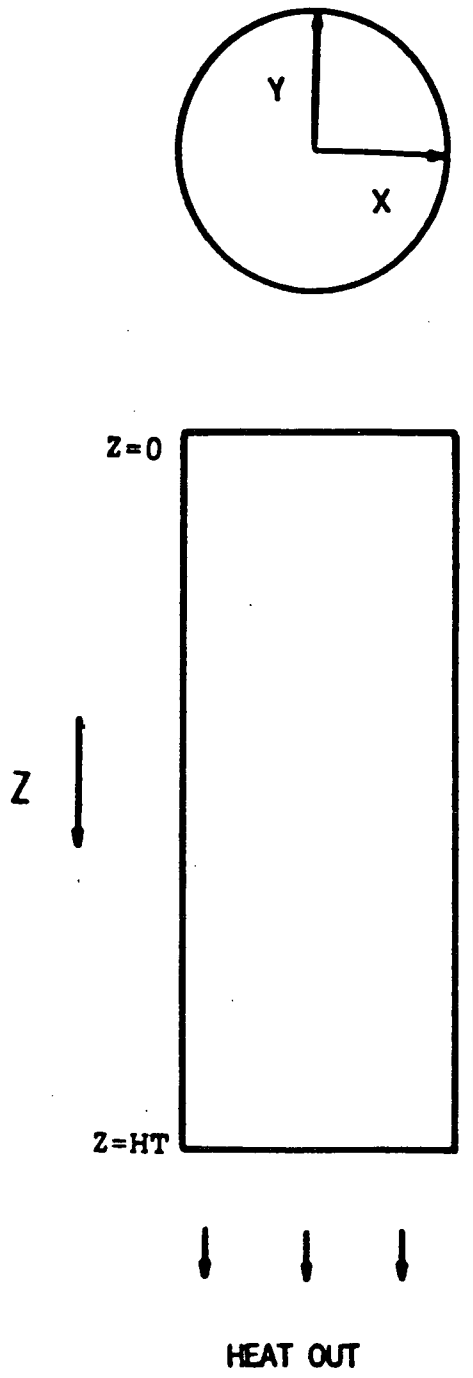

Figure 14 - Coordinates used in casting.

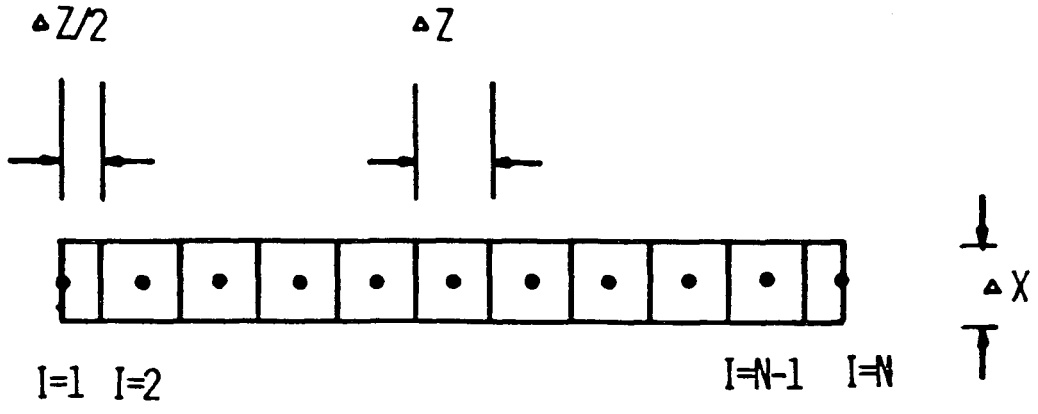

Figure 15 - Arrangement of nodes in the finite difference calculations.

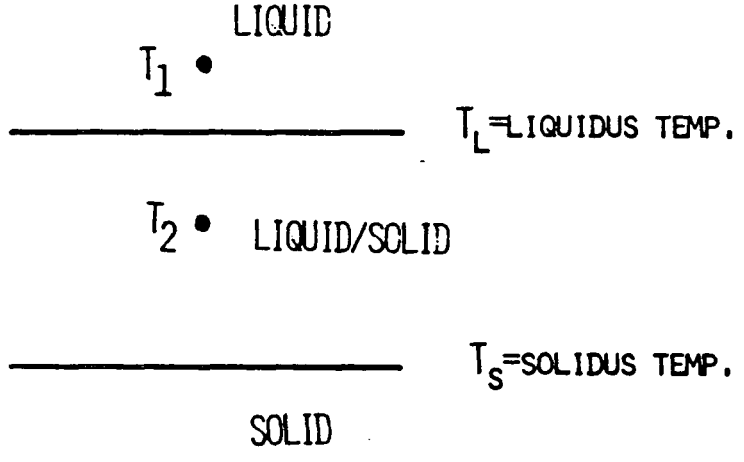

Figure 16 - Correction of a nodal temperature for a node jumping from above the liquidus to the solid/liquid region.

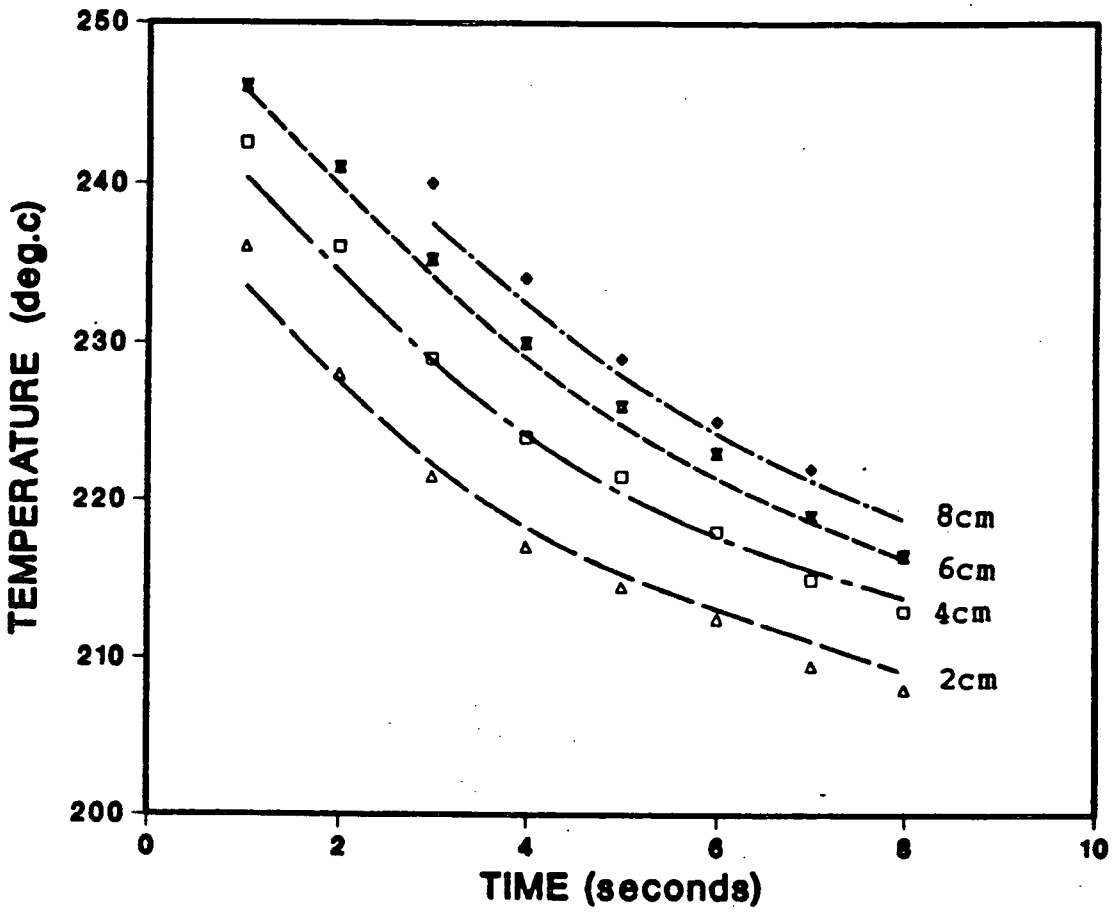

Figure 17 - Comparison of the calculated and measured temperatures during solidification, at different positions in the melt.

a b

Figure 18 - (a-b) Typical structures of samples showing columnar grains, equiaxed grains, and a horizontal columnar to equiaxed transition. Mag 1.5X

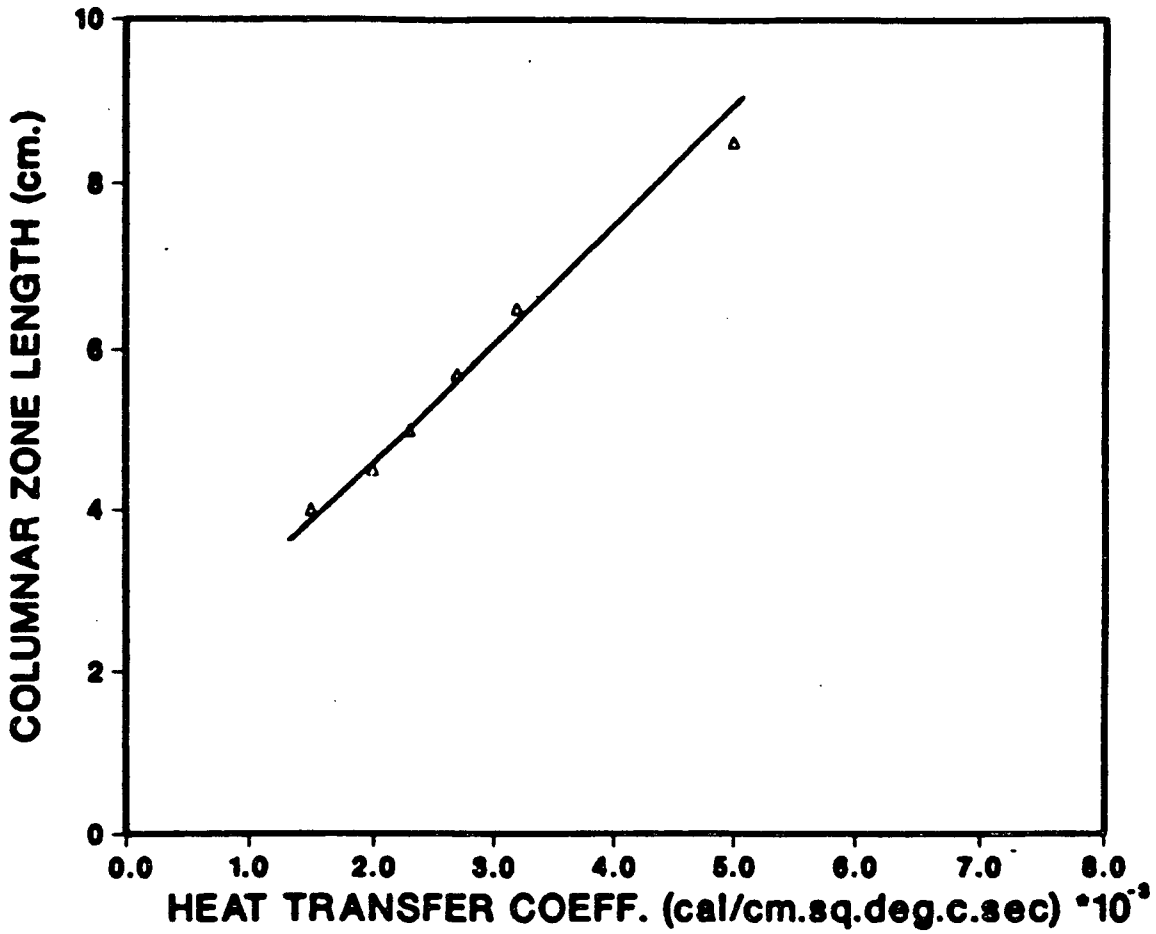

Figure 19 - Columnar zone length as a function of heat transfer coefficient for Sn-10wt%Pb.

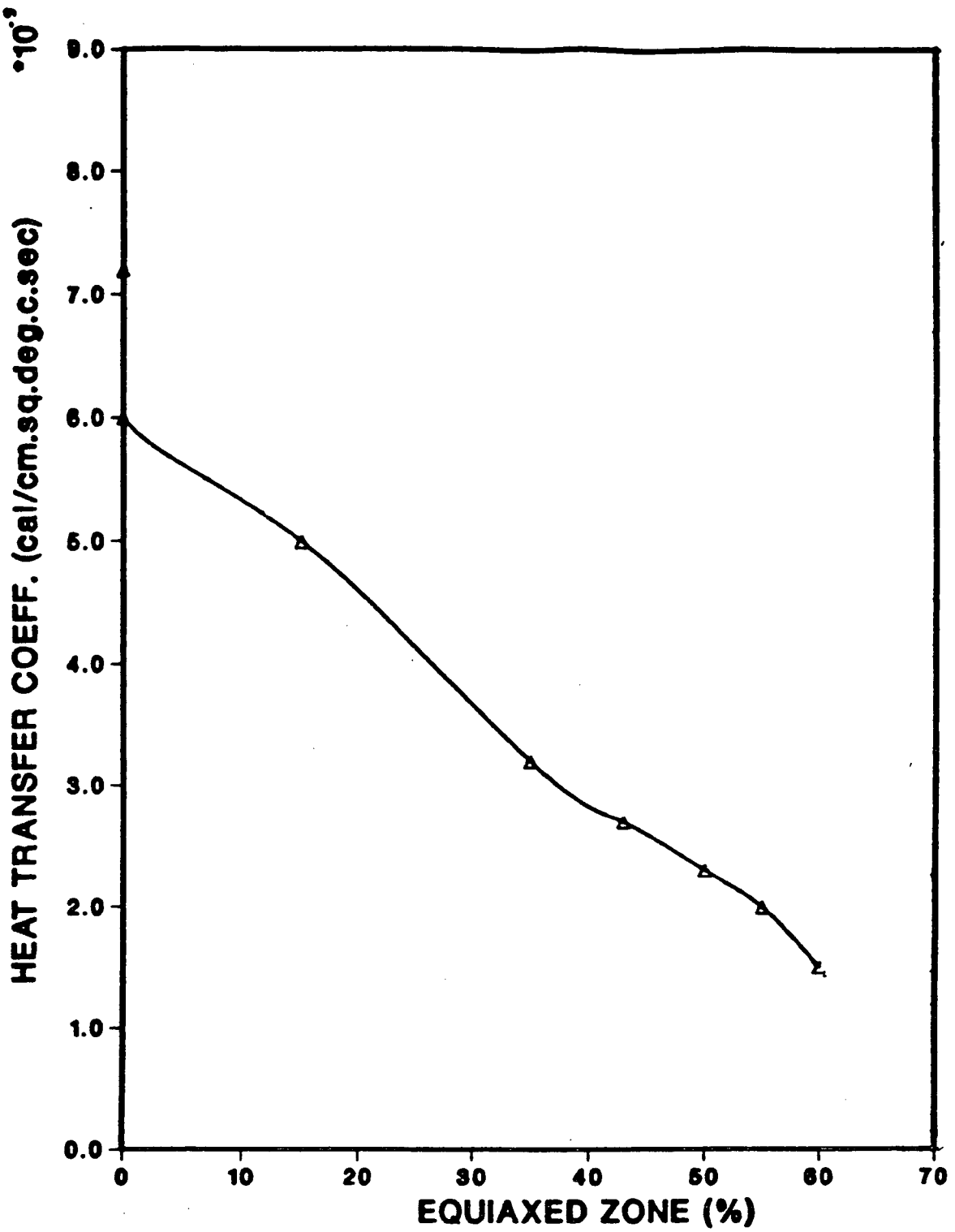

Figure 20 - Variation of percent equiaxed zone with heat transfer coefficients for Sn-10wt%Pb.

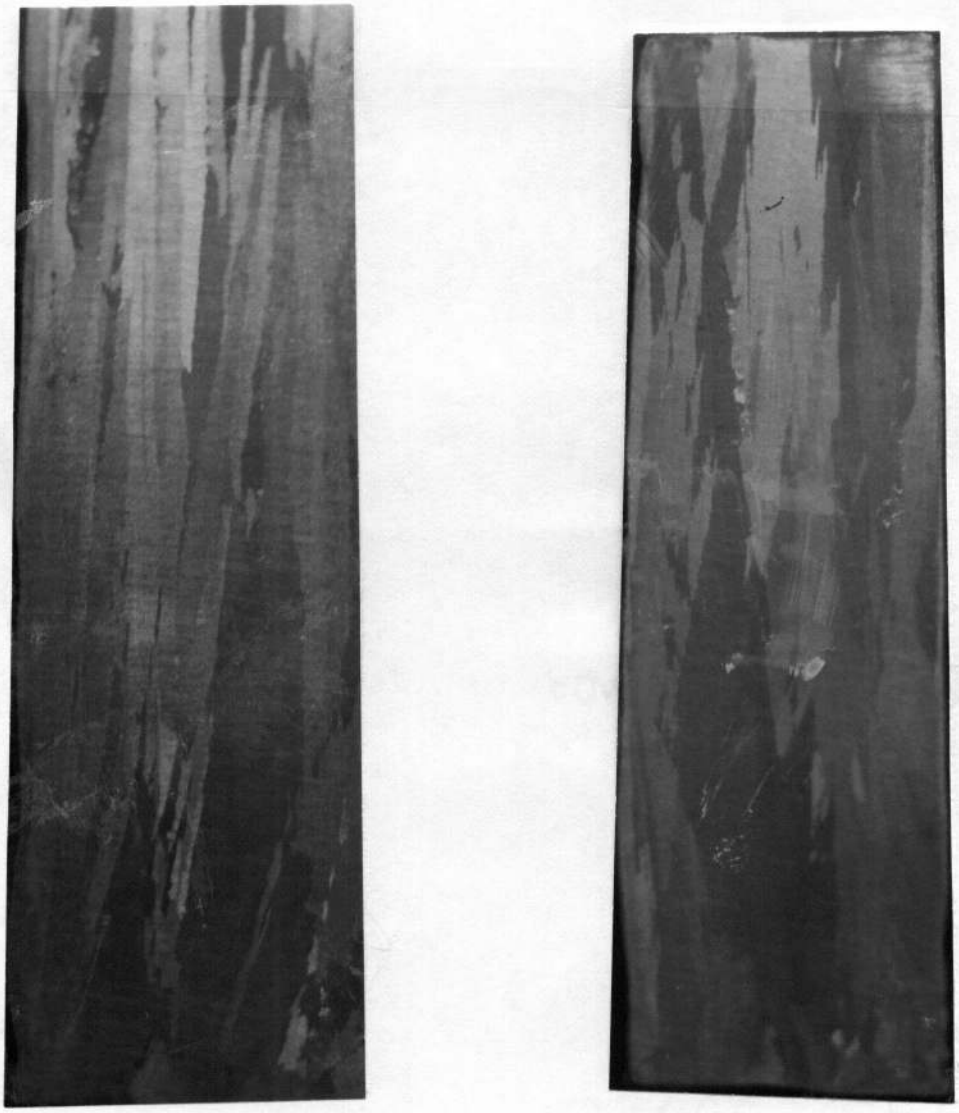

Figure 21 - Samples showing no columnar to equiaxed transition and consisting of entirely columnar grains. Mag 1.5X

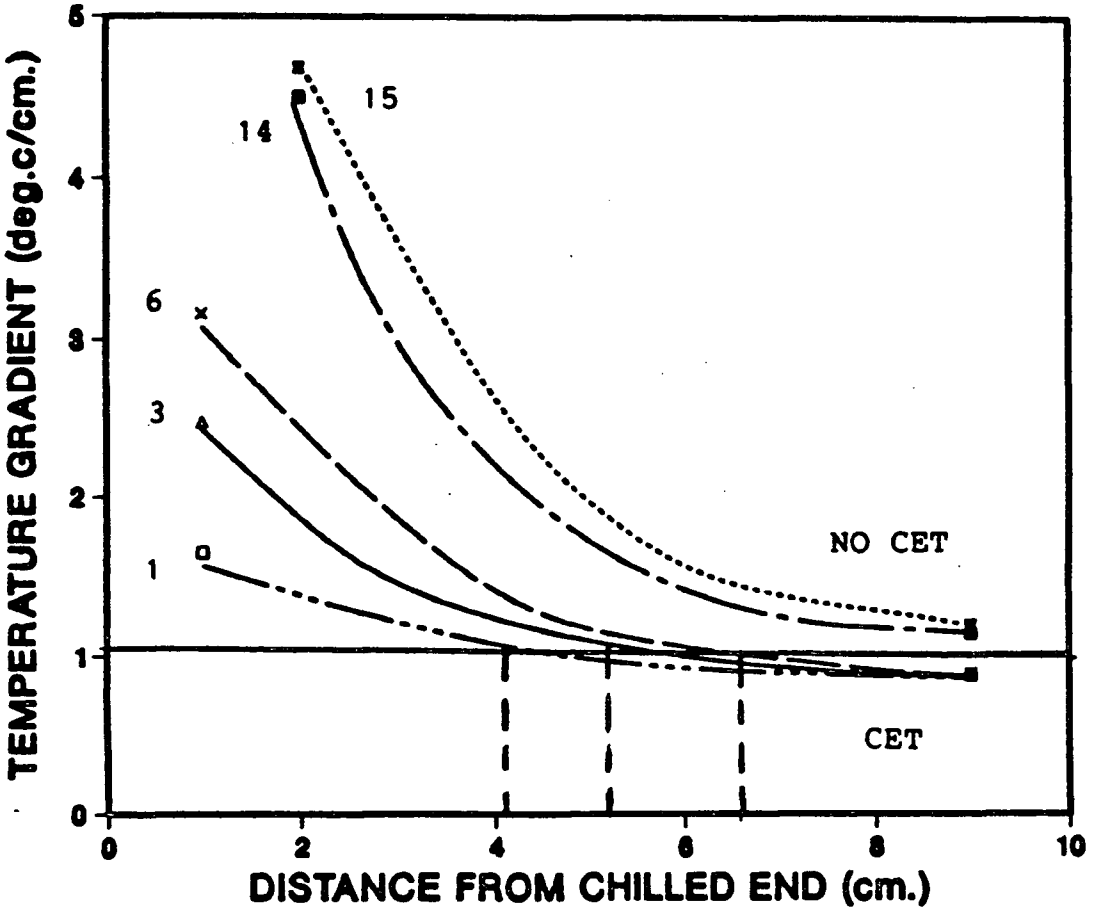

Figure 22 - Variation of temperature gradient in the melt as a function of the distance from the chilled end for Sn-10%Pb alloy. where H=heat transfer coefficient.

Test 1 H=0.0023, Test 3 H=0.0015, Test 6 H=0.0032, Test 14 H=0.0060, Test 15 H=0.0072

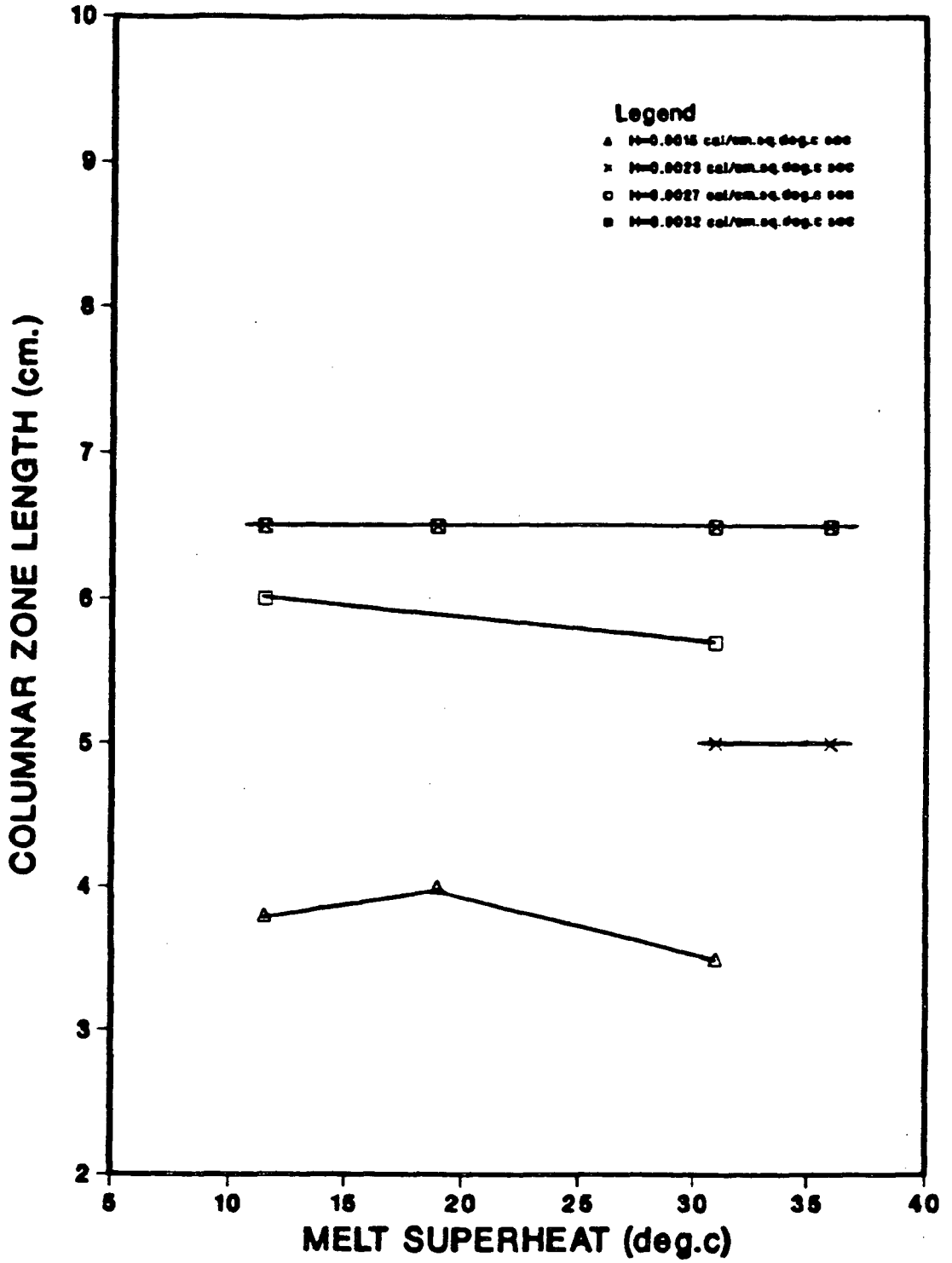

Figure 23 - Variation of columnar zone length as a function of melt superheat for different heat transfer coefficients, H in Sn-10%wtPb.

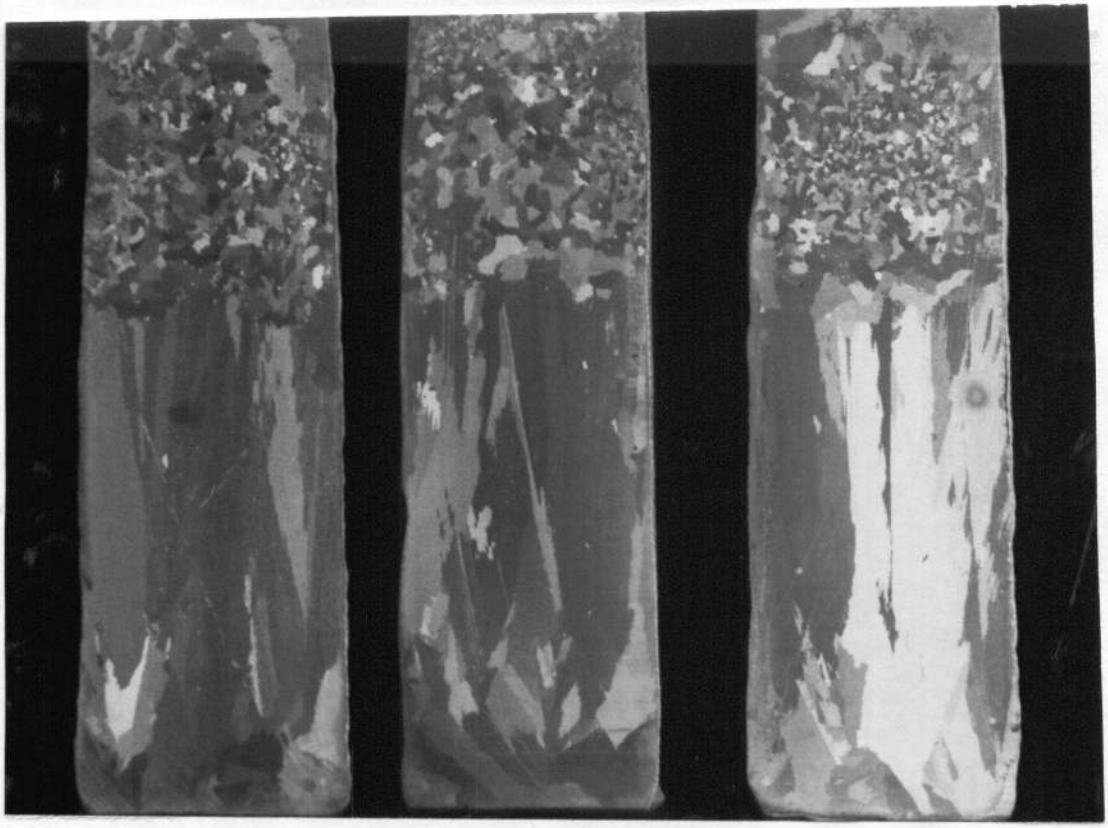

(a) (b) (c)

SUPERHEAT=36 DEG.C SUPERHEAT=31 DEG.C SUPERHEAT=19 DEG.C

Figure 24 - Photographs of three samples cast with different superheats, but cooled identically having the same columnar zone length.

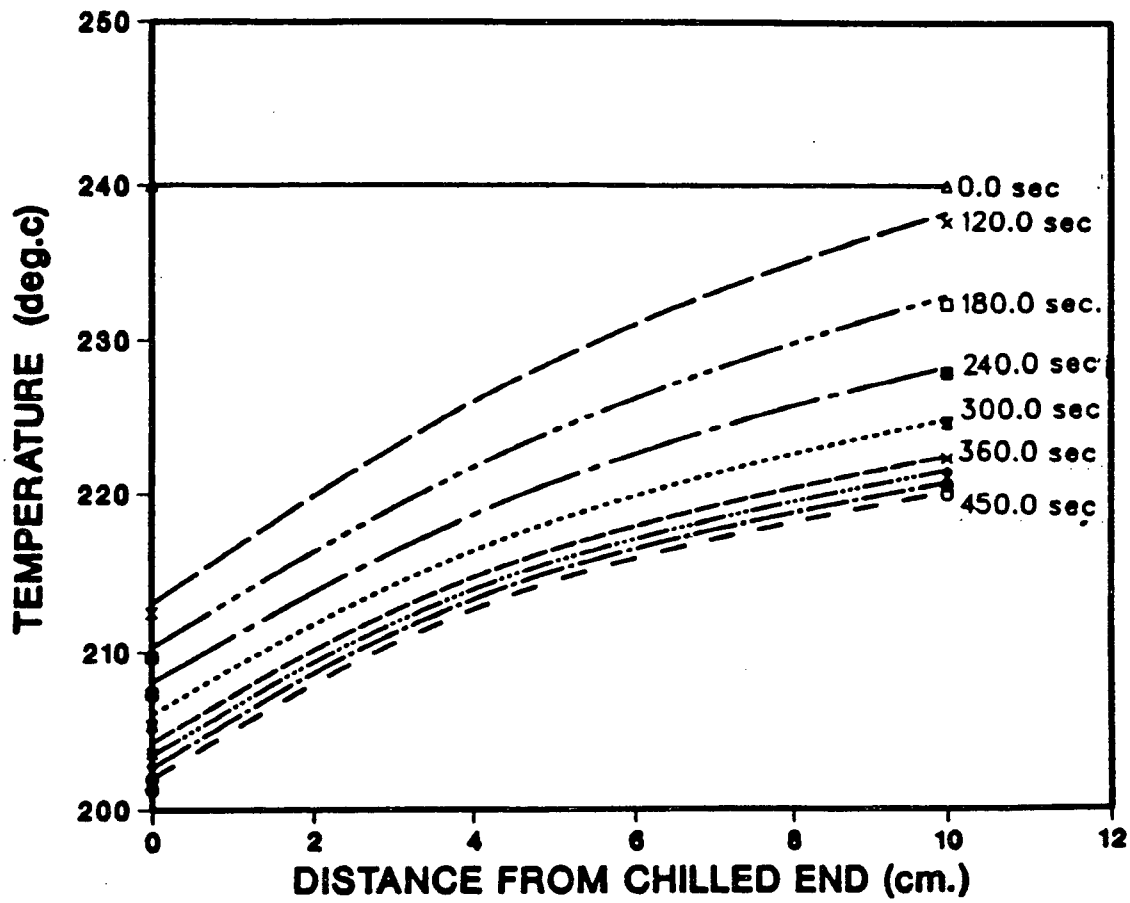

Figure 25 - The temperature distribution as a function of distance from the chill end at the times indicated.

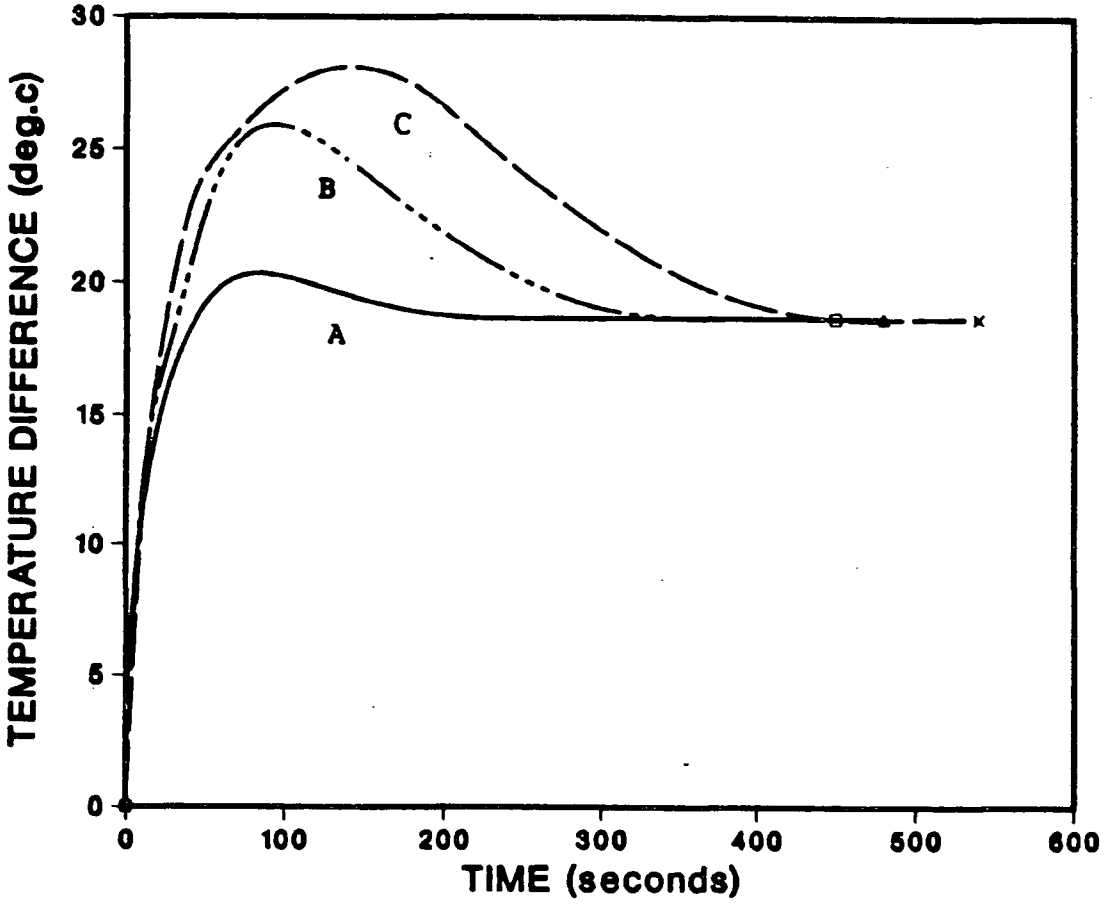

Figure 26 - The temperature difference between the chill face and sample end as a function of time for the three initial superheats indicated.

A-Superheat=15.0°C B-Superheat=25.0°C C-Superheat=35.0°C

Figure 27 - Photograph of the sample cast with Fe powder addition in melt. Mag 1.8X.

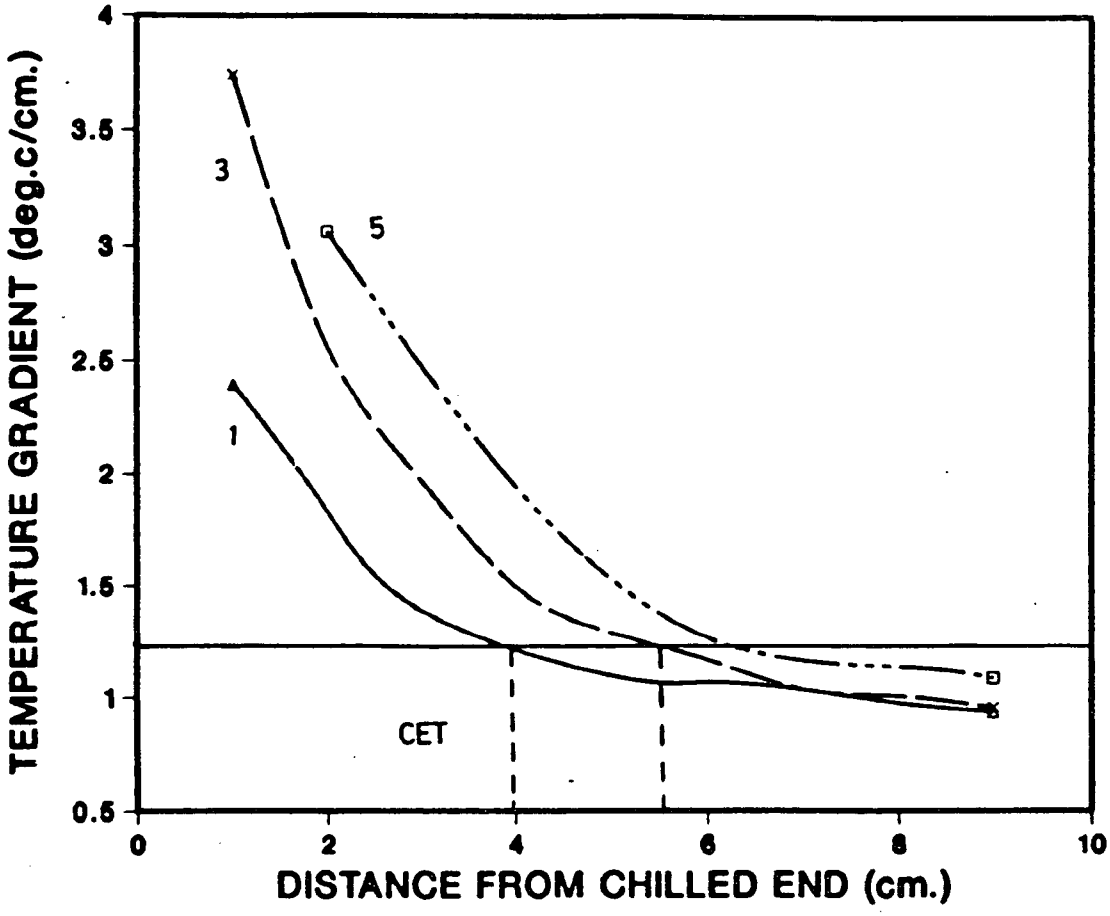

Figure 28 - Variation of the temperature gradient in the melt as a function of the distance from the chill end for Sn-15wt%Pb alloy.

Test 1 H=0.0025, Test 3 H=0.0040, Test 5 H=0.0065

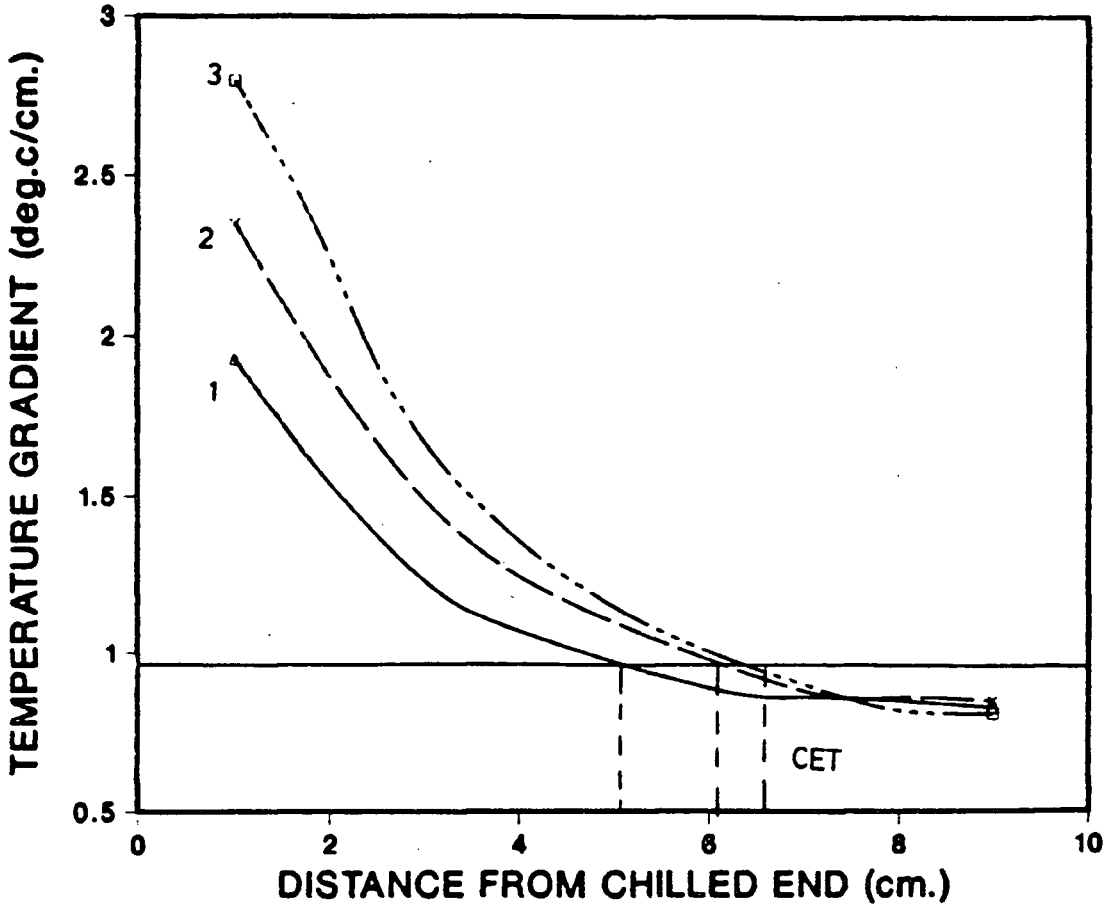

Figure 29 - Variation of the temperature gradient in the melt as a function of the distance from the chill end for Sn-5wt%Pb alloy.

Test 1 H=0.0017, Test 2 H=0.0022, Test 3 H=0.0027

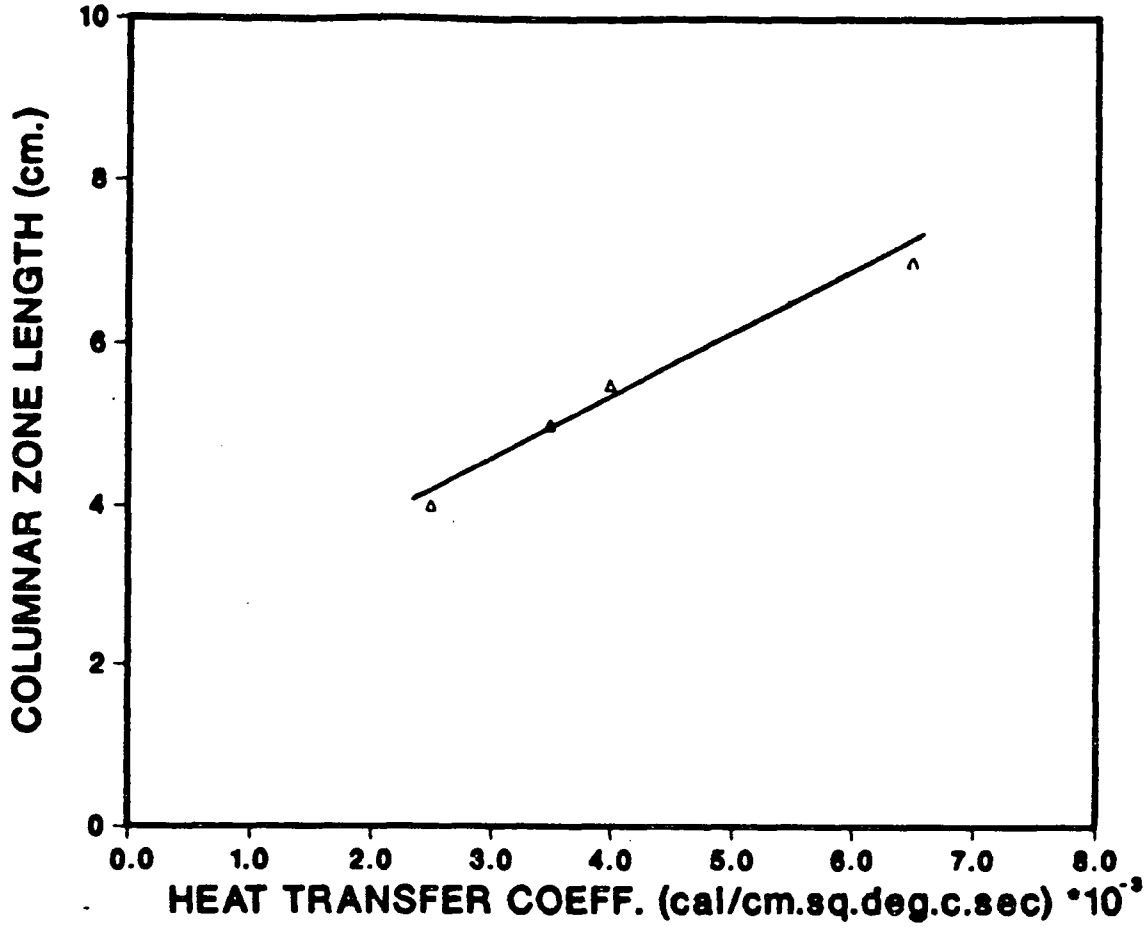

Figure 30 - Variation of the columnar zone length as a function of the heat transfer coefficient for Sn-15wt%Pb alloy.

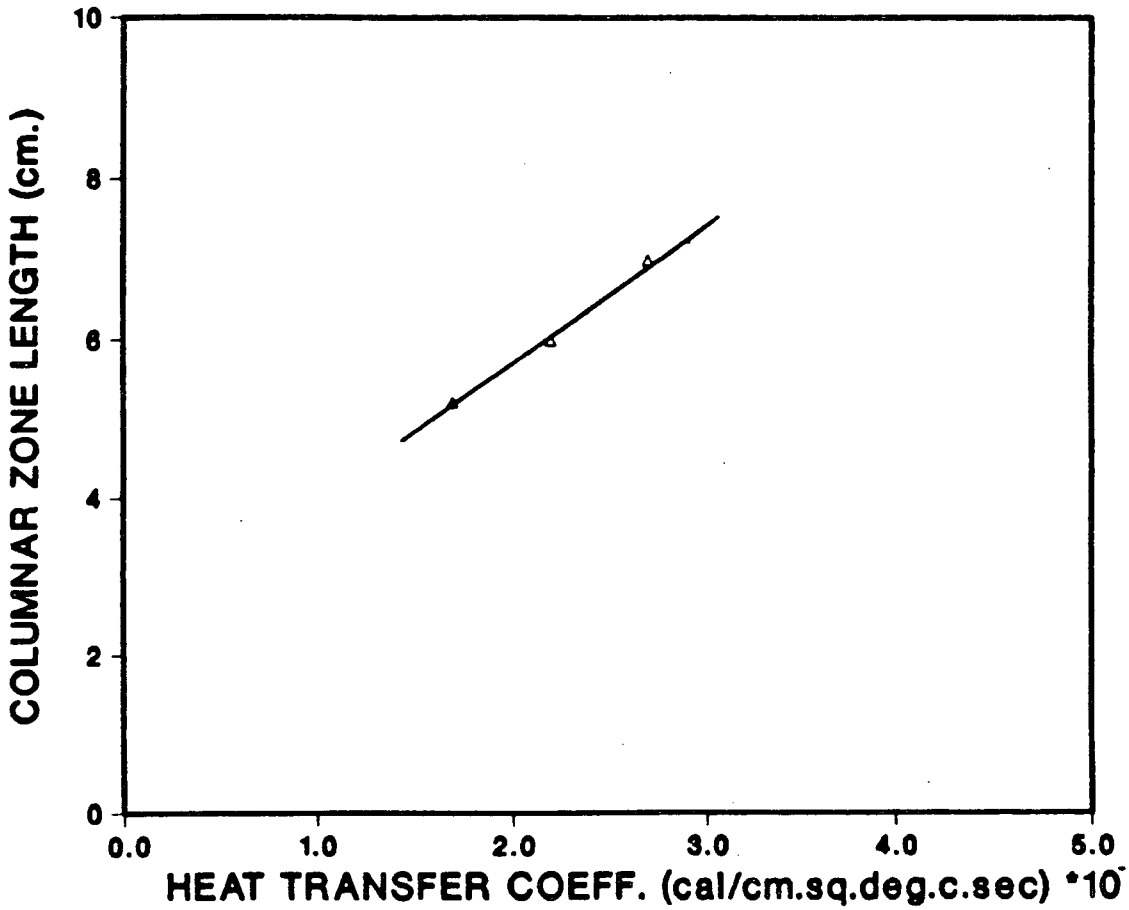

Figure 31 - Variation of the columnar zone length as a function of the heat transfer coefficient for Sn-5wt%Pb alloy.

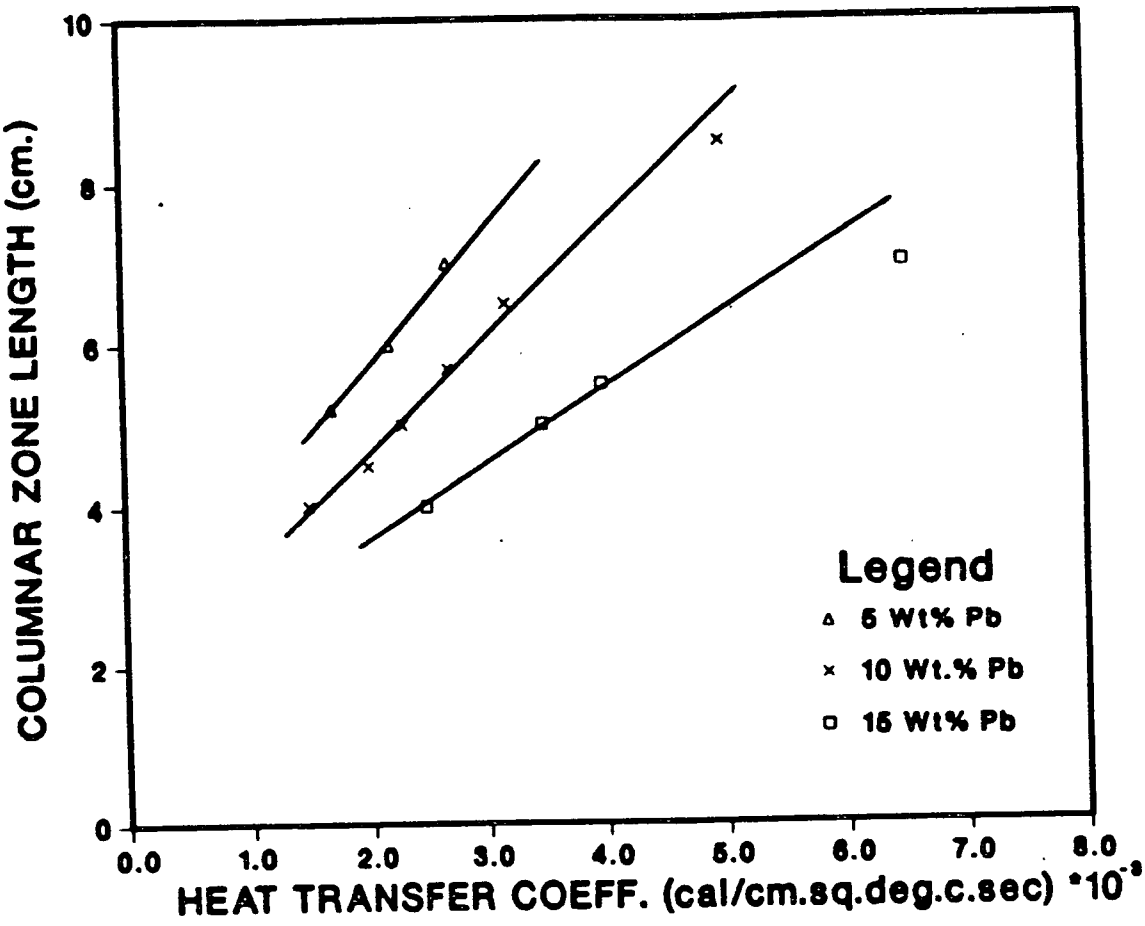

Figure 32 - Variation of the columnar zone length as a function of the heat transfer coefficient for 5, 10 and 15wt%Pb.

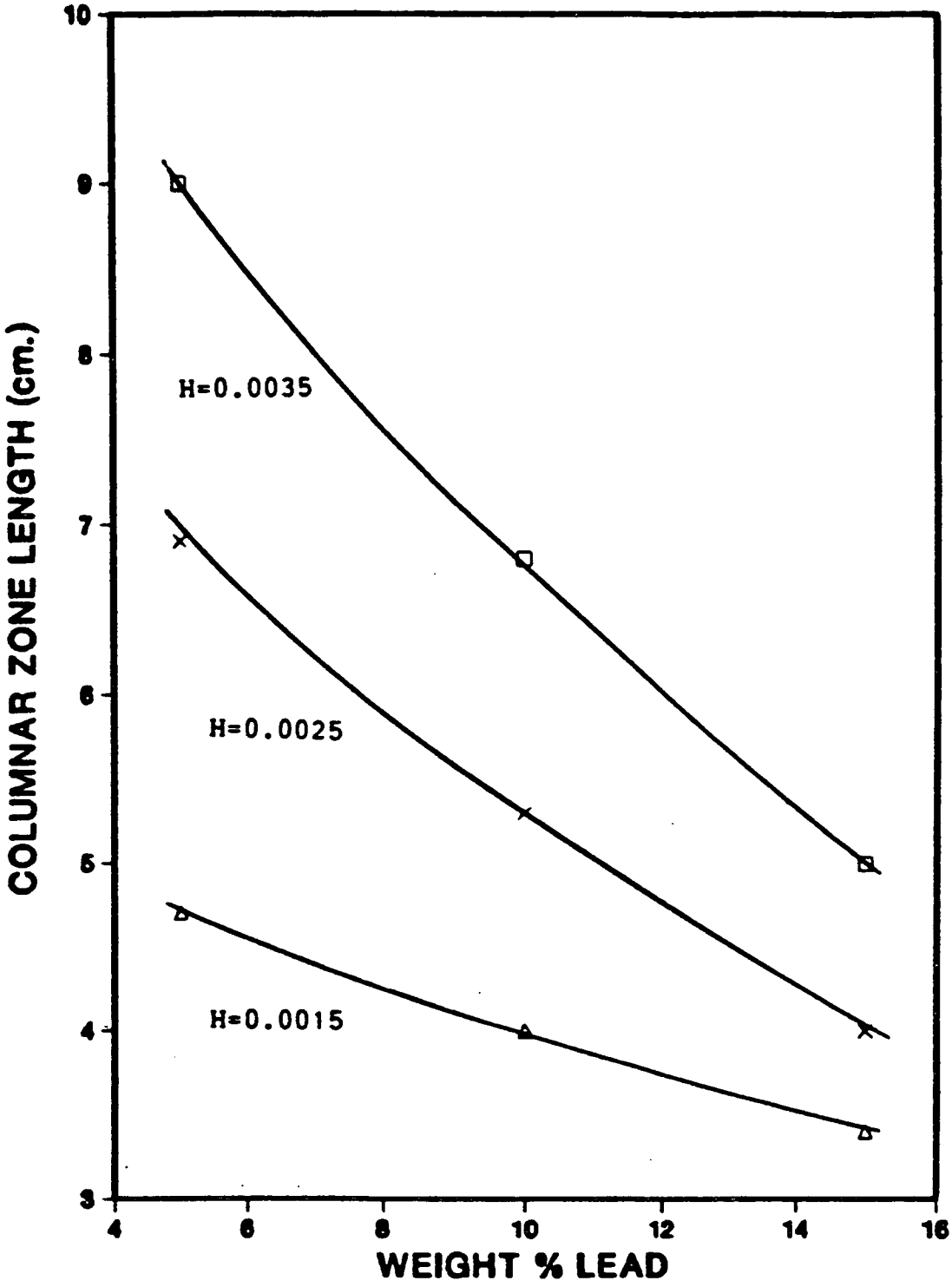

Figure 33 - Variation of the columnar zone length as a function the Pb content of Sn-Pb alloy.

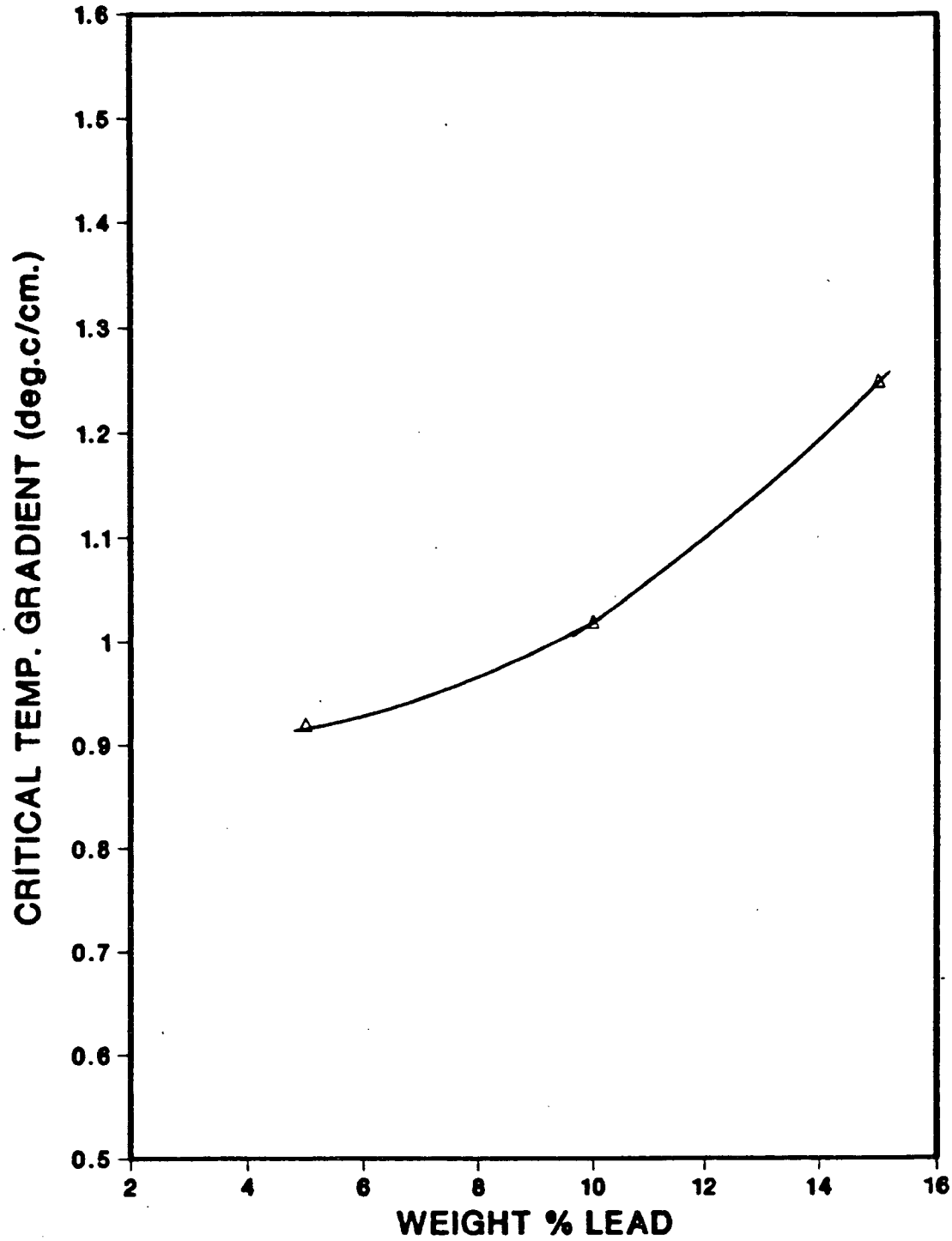

Figure 34 - Critical temperature gradient for the columnar to equiaxed transition for different Pb contents in Sn-Pb alloy.

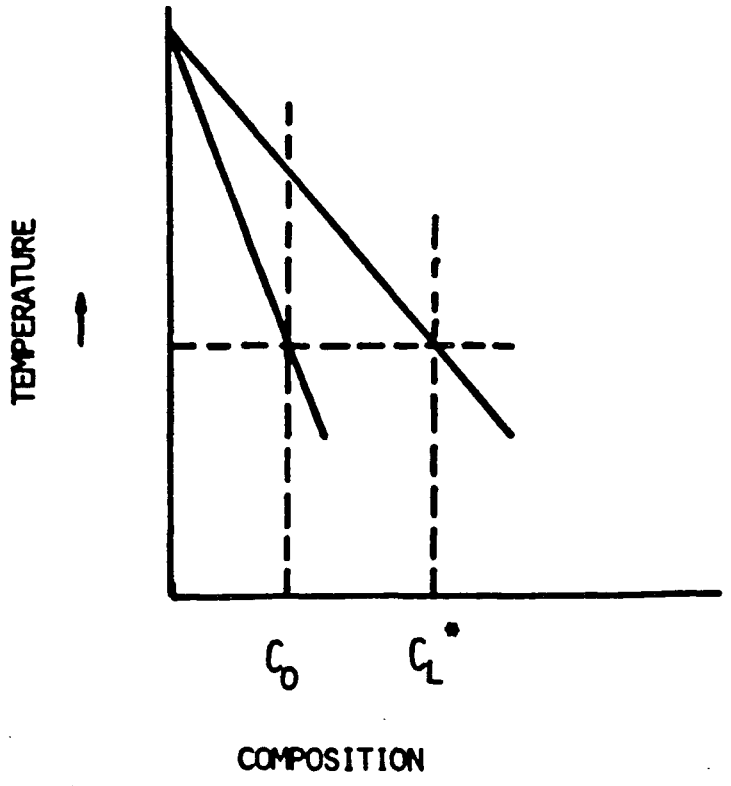

Figure 35 - Solidification of an alloy of composition C_o.

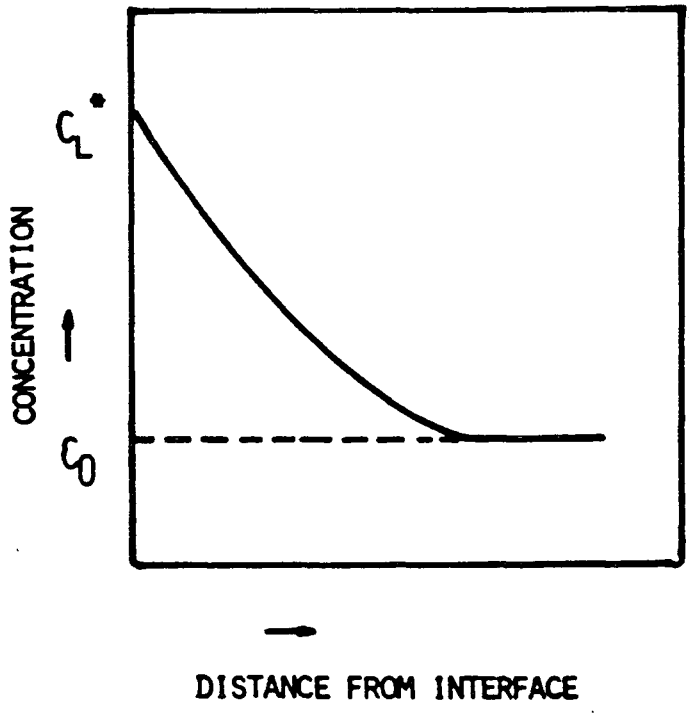

Figure 36 - Schematic description of the liquid composition in the melt ahead of a flat solid/liquid interface.

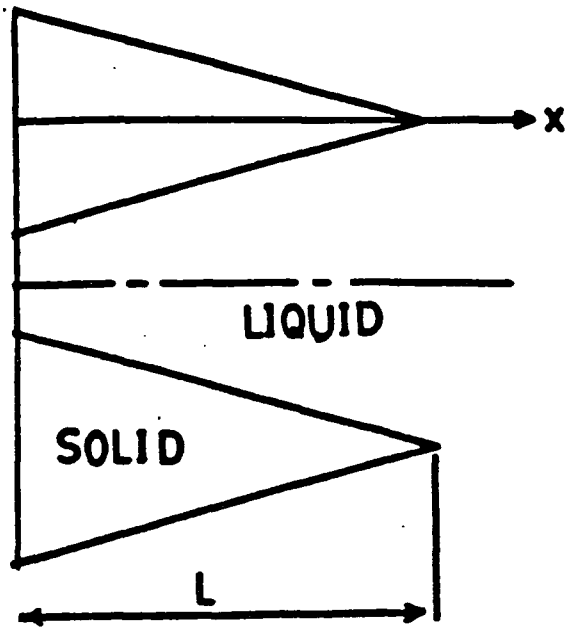

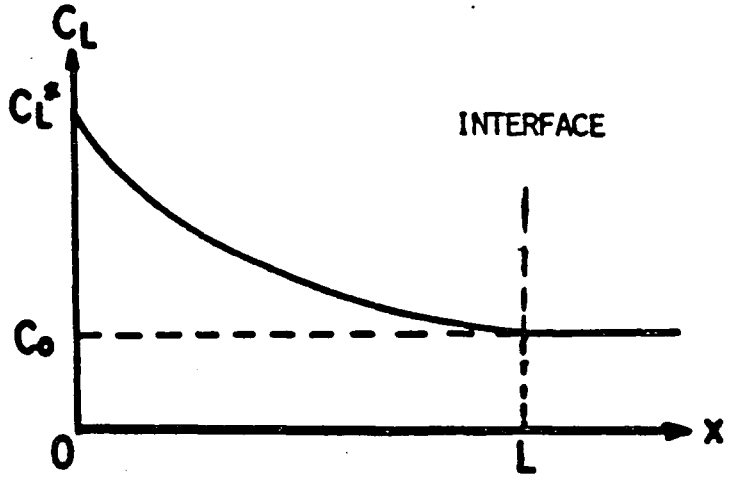

Figure 37 - Schematic description of the liquid composition ahead of a columnar dendritic interface

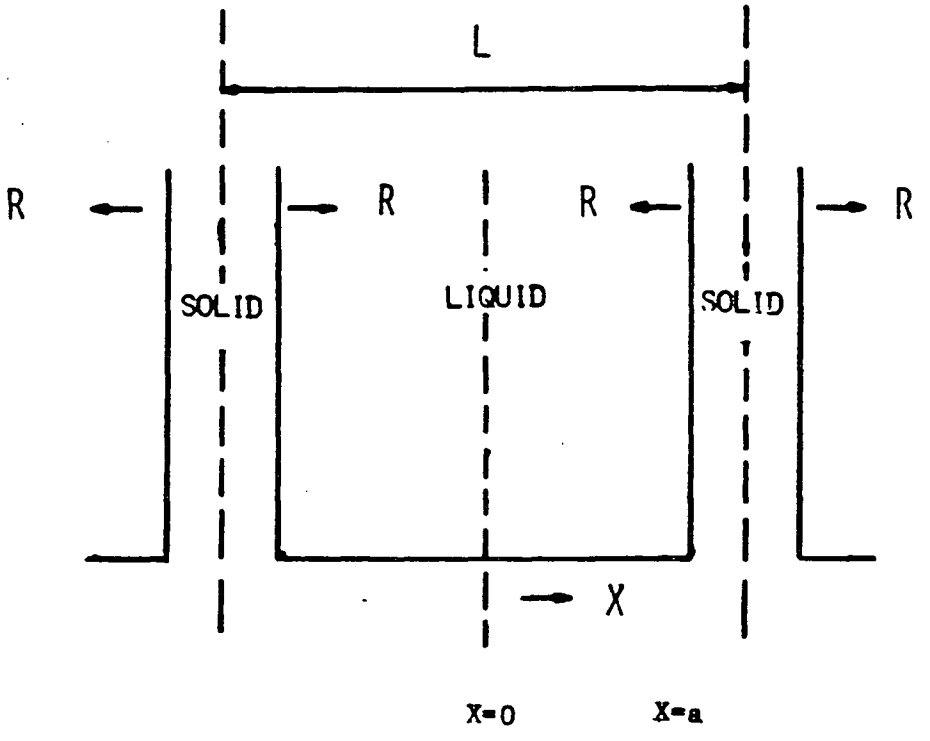

Figure 38 - Schematic drawing of two primary dendrites represented by two parallel flat plates.

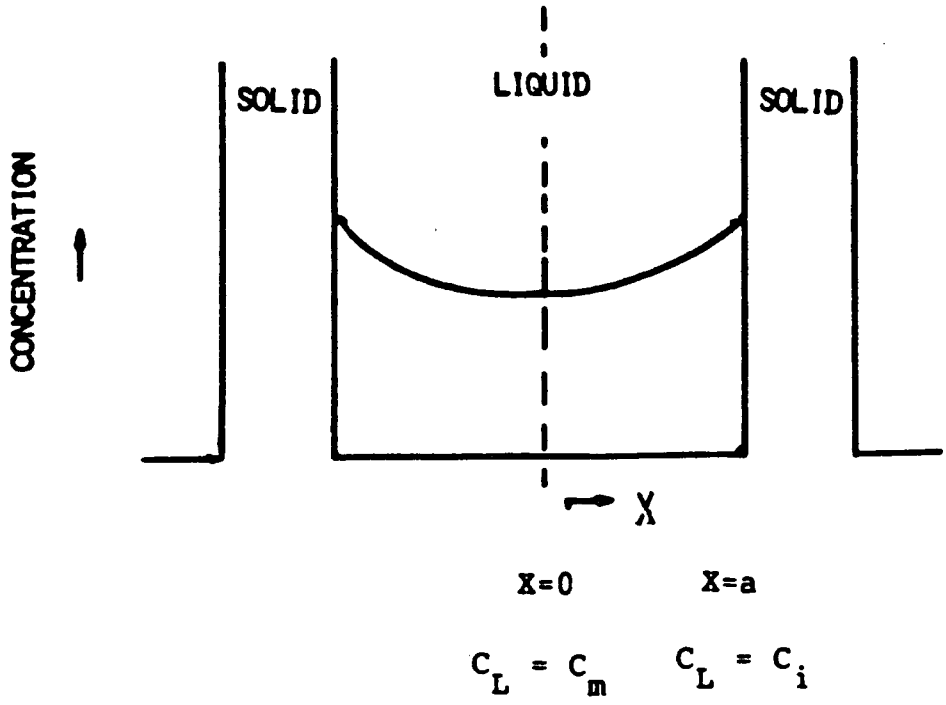

Figure 39 - Schematic representation of the liquid composition in the interdendritic region.

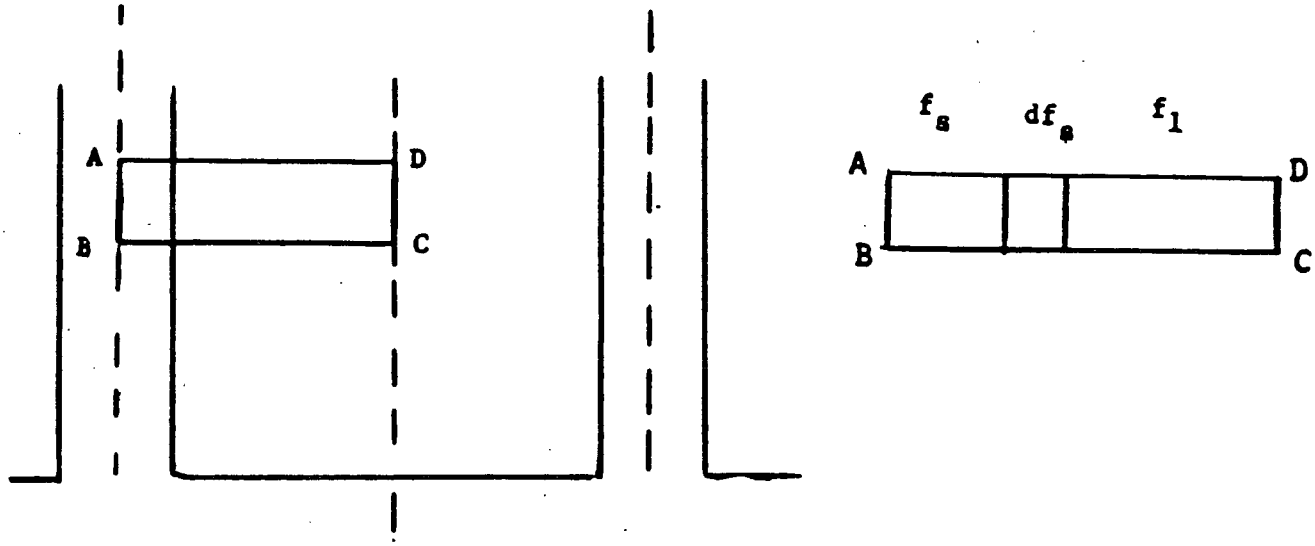

Figure 40 - Transverse section across a primary dendrites showing fraction solid and fraction liquid.

Figure 41 - Photograph of sample cast with radioactive tracer

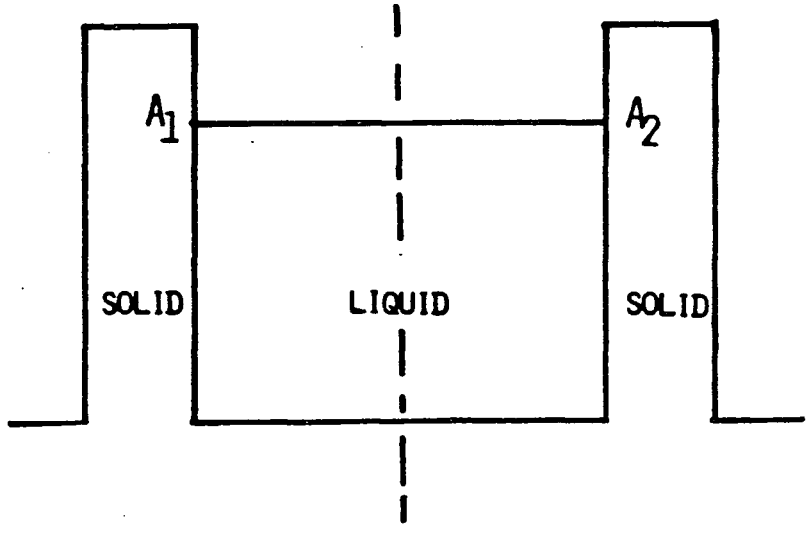

Figure 42 - The position in the liquid, along $A_1 A_2$ in the interdendritic region where the composition has been calculated.

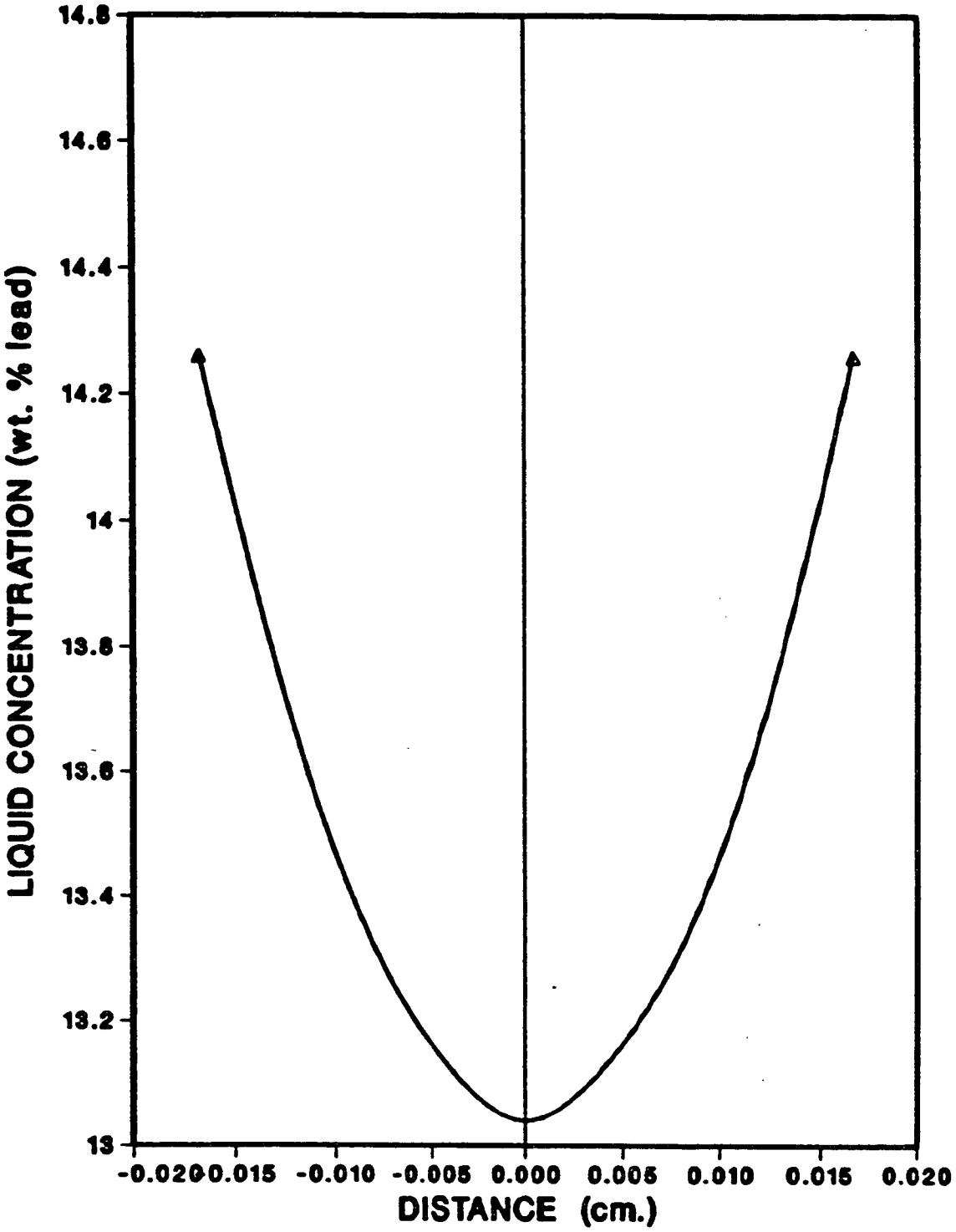

Figure 43 - Calculated liquid composition along A_1A_2. Distance=0.0 denotes the centre of the interdendritic region.

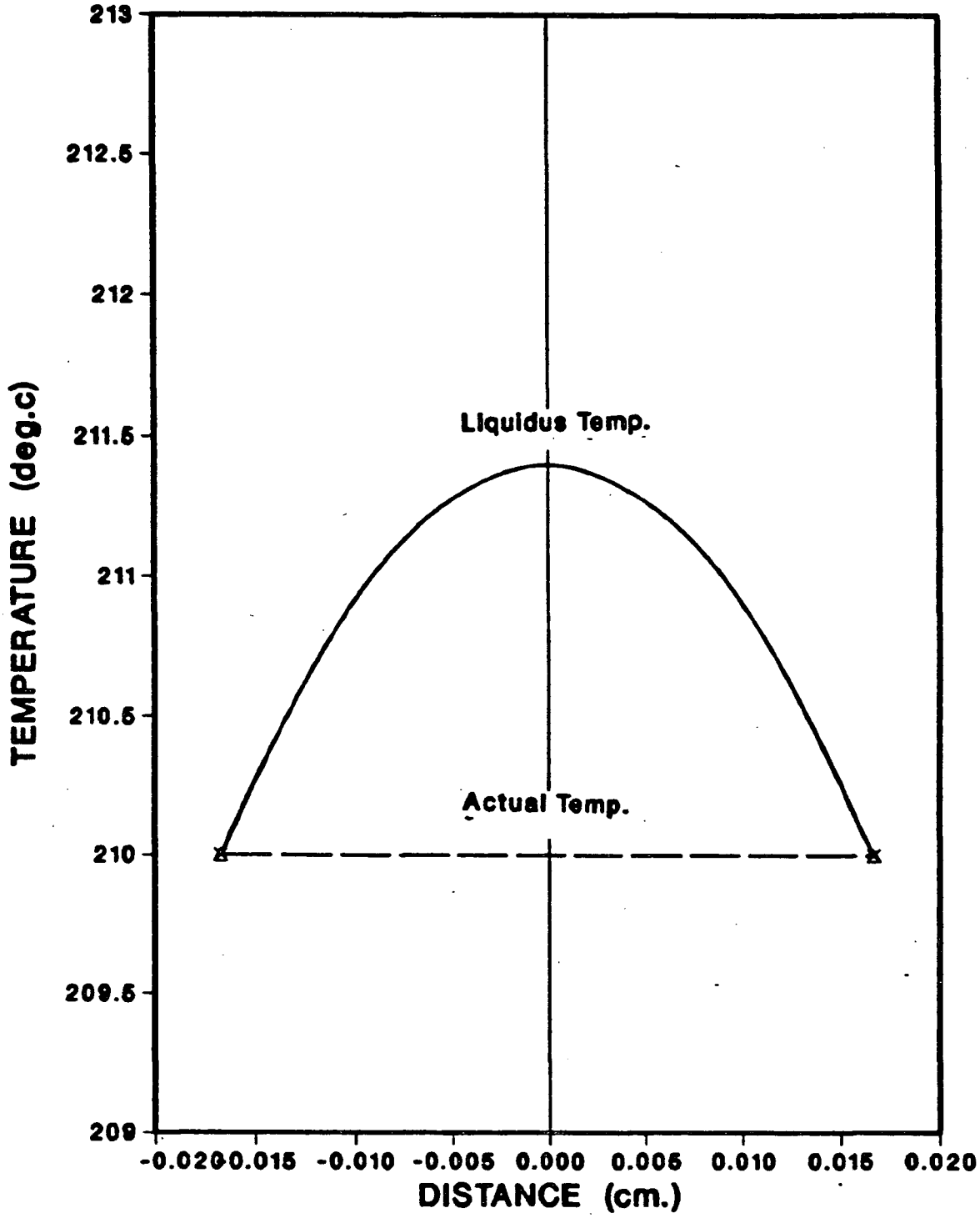

Figure 44 - Interdendritic region where constitutional supercooling occurs, Distance=0.0 denotes the centre of the interdendritic region.

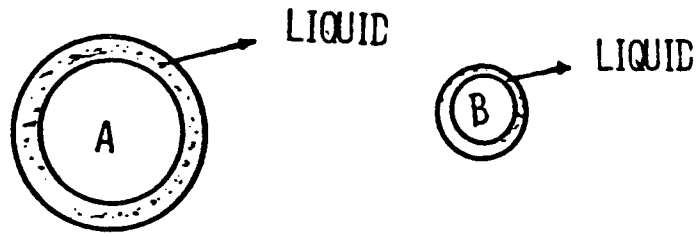

Figure 45 - Competitive growth between a columnar dendrite A and a nucleus B.

Table I
Results for the Sn-10wt%Pb alloy

Test No.	Initial Temp. °C	Superheat °C	Heat transfer Coefficient Cal/cm²°CSec	CET	Position of CET cm
1	251.0	36.0	0.0023	yes	5.0
2	251.0	36.0	0.0032	yes	6.5
3	246.0	31.0	0.0015	yes	3.5
4	246.0	31.0	0.0023	yes	5.0
5	246.0	31.0	0.0027	yes	5.7
6	246.0	31.0	0.0032	yes	6.5
7	234.0	19.0	0.0015	yes	4.0
8	234.0	19.0	0.0020	yes	4.5
9	234.0	19.0	0.0032	yes	6.5
10	226.5	11.5	0.0015	yes	3.8
11	226.5	11.5	0.0027	yes	6.0
12	226.5	11.5	0.0032	yes	6.5
13	251.0	36.0	0.0050	yes	8.0
14	246.0	31.0	0.0060	no	-
15	256.0	41.0	0.0072	no	-

Table II
Temperature gradient in the melt at different positions for the Sn-10wt%Pb alloy.

Test No.	Initial Temp. °C	Hx10⁻¹	(dT/dx)°C/cm different distances from the chilled end(cm)									(dT/dx) CET
			1.0	2.0	3.0	4.0	5.0	6.0	7.0	8.0	9.0	
1	251.0	0.23	2.48	1.90	1.40	1.18	1.01	0.98	0.97	0.93	0.90	1.01
2	251.0	0.32	3.16	2.42	1.82	1.37	1.16	1.05	0.98	0.97	0.93	1.02
3	246.0	0.15	1.65	1.39	1.17	1.01	0.95	0.93	0.92	0.91	0.89	1.01
4	246.0	0.23	2.30	1.75	1.40	1.19	1.01	0.99	0.97	0.94	0.90	1.01
5	246.0	0.27	2.78	2.02	1.55	1.22	1.16	1.02	0.95	0.93	0.92	1.03
6	246.0	0.32	3.40	2.47	1.86	1.40	1.17	1.07	0.99	0.93	0.90	1.03
7	234.0	0.15	1.65	1.39	1.16	1.06	0.99	0.94	0.92	0.90	0.88	1.06
8	234.0	0.20	2.10	1.70	1.34	1.08	1.03	0.98	0.95	0.90	0.89	1.05
9	234.0	0.32	3.19	2.77	1.84	1.32	1.14	1.03	1.01	0.93	0.89	1.02
10	226.5	0.15	1.65	1.36	1.17	1.01	0.98	0.97	0.95	0.93	0.90	1.03
11	226.5	0.27	2.80	2.05	1.62	1.30	1.14	0.99	0.95	0.91	0.90	0.99
12	226.5	0.32	2.98	2.12	1.76	1.30	1.16	1.06	0.98	0.93	0.89	1.02

Table III
Temperature gradient in the melt at different positions in experiments where the columnar to equiaxed transition could not be obtained

Test No.	Initial Temp. °C	Hx10⁻¹	(dT/dx)°C/cm different distances from the chilled end(cm)								
			1.0	2.0	3.0	4.0	5.0	6.0	7.0	8.0	9.0
14	246.0	0.60	6.12	4.50	2.88	2.20	1.64	1.54	1.28	1.22	1.15
15	256.0	0.72	6.85	4.68	3.80	2.69	1.99	1.57	1.39	1.30	1.20

H is in Cal/cm²°C.sec

Table IV
Effect of superheat on columnar zone length for Sn-10wt%Pb alloy

Test No.	Initial Temp. °C	Superheat °C	Heat transfer coefficient Cal/cm²°CSec	Columnar zone length
1	226.5	11.5	0.0015	3.8
2	234.0	19.0	0.0015	4.0
3	246.0	31.0	0.0015	3.5
4	246.0	31.0	0.0023	5.0
5	251.0	36.0	0.0023	5.0
6	226.5	11.5	0.0027	6.0
7	246.0	31.0	0.0027	5.7
8	226.5	11.5	0.0032	6.5
9	234.0	19.0	0.0032	6.5
10	246.0	31.0	0.0032	6.5
11	251.0	36.0	0.0032	6.5

Table V
Temperature gradient in the melt at different positions for experiments done with Fe powder additions.

Test No.	Initial Temp. °C	Heat transfer coefficient Cal/cm²°CSec	Transition	Position of (CET)	(dT/dx) CET	Remarks
5	246.0	0.0027	yes	5.7	1.03	
14	246.0	0.0060	no	-	-	Minimum temp gradient in the melt was 1.15°C/cm

Table VII
Temperature gradient in the melt at different positions for the Sn-15%Pb alloy

Test No.	Initial Temp °C	Hx10⁻¹	(dT/dx)°C/cm different distances from the chilled end(cm) 1.0	2.0	3.0	4.0	5.0	6.0	7.0	8.0	9.0	(dT/dx) CET
1	246.0	0.25	2.38	1.83	1.39	1.28	1.10	1.07	1.04	0.98	0.94	1.28
2	251.0	0.35	3.53	2.39	1.77	1.46	1.25	1.10	1.07	0.99	0.96	1.25
3	231.5	0.36	3.41	2.48	1.98	1.43	1.26	1.20	1.10	1.05	0.99	1.26
4	231.5	0.40	3.74	2.56	1.97	1.50	1.29	1.17	1.04	1.01	0.96	1.23
5	231.5	0.65	5.20	3.06	2.06	1.95	1.40	1.27	1.23	1.14	1.09	1.23

Table IX
Temperature gradient in the melt at different positions for the Sn-5wt% Pb alloy

Test No.	Initial Temp. °C	Hx10⁻¹	(dT/dx)°C/cm different distances from the chilled end(cm) 1.0	2.0	3.0	4.0	5.0	6.0	7.0	8.0	9.0	(dT/dx) CET
1	231.5	0.17	1.93	1.54	1.23	1.07	1.02	0.89	0.86	0.85	0.83	0.94
2	236.0	0.22	2.35	2.00	1.49	1.28	1.10	0.91	0.88	0.86	0.85	0.91
3	246.0	0.27	2.80	2.25	1.67	1.40	1.15	1.06	0.90	0.88	0.86	0.90

H is in Cal/cm²°C.sec

Table VI
Results for the Sn-15wt%Pb alloy

Test No.	Initial Temp. °C	Superheat °C	Heat transfer Coefficient Cal/cm²°CSec	CET	Position of CET
1	246.0	36.0	0.0025	yes	4.0
2	251.0	41.0	0.0035	yes	5.0
3	231.5	21.5	0.0036	yes	4.8
4	231.5	21.5	0.0040	yes	5.5
5	231.5	21.5	0.0065	yes	7.0

Table VIII
Results for the Sn-5wt%Pb alloy

Test No.	Initial Temp. °C	Superheat °C	Heat transfer Coefficient Cal/cm²°CSec	CET	Position of CET
1	231.5	7.5	0.0017	yes	5.2
2	236.0	12.0	0.0022	yes	6.0
3	246.5	22.0	0.0027	yes	7.0
4	236.0	12.0	0.0035	no	-

Table X
Critical temperature gradient for the columnar to equiaxed transition for Sn-5, 10 & 15wt% Pb

Pb %Wt	$(dT/dx)_{CET}$ °C/cm
5	0.92
10	1.02
15	1.25

Table XI
Interdendrite liquid composition at different distances from the centre of the interdentritic region.

Distance	0.0 cm	4.16×10^{-3} cm	8.33×10^{-3} cm	1.25×10^{-2} cm	1.67×10^{-2} cm
Comp. (Pb%)	13.04	13.12	13.34	13.72	14.26

Table XII
Maximum supercooling in the interdendritic region for different Pb contents

Pb wt%	ΔC	ΔT °C
5	0.61	1.03
10	1.22	1.40
15	1.84	2.07

7. APPENDIX A -DERIVATION OF NODAL EQUATIONS

The partial differential equation for one dimentional Transient problem (equation 7) and boundary conditions were solved using implicit finite difference technique. Fig15 shows the arrangement of nodes. The nodal equations are obtained by applying heat balance on each node as given below.

a) Top node I=1

$$\frac{k(T'_{I+1}-T'_I)}{\Delta x}\Delta x = \frac{\rho C\Delta x^2}{2}\frac{(T'_I - T_I)}{\Delta t}$$

$$-(2k + \frac{\rho C\Delta x^2}{\Delta t})T'_I + 2kT'_{I+1} = -\frac{\rho C\Delta x^2}{\Delta t}T_I \qquad 1$$

b) Interior node: I=2,.....N-1

$$\frac{k(T'_{I-1}-T'_I)}{\Delta x}\Delta x + \frac{k(T'_{I+1}-T'_I)}{\Delta x}\Delta x = \rho C\Delta x^2\frac{(T'_I - T_I)}{\Delta t}$$

$$kT'_{I-1} - (2k + \frac{\rho C\Delta x^2}{\Delta t})T'_I + kT'_{I+1} = -\frac{\rho C\Delta x^2}{\Delta t}T_I \qquad 2$$

c) Bottom node, I=N

$$\frac{k(T'_I - T'_{I-1})}{\Delta x}\Delta x - H\Delta x(T'_I - T_a) = \frac{\rho C\Delta x^2}{2}\frac{(T'_I - T_I)}{\Delta t}$$

$$-2kT'_{I-1} - (2k+2H + \frac{\rho C\Delta x^2}{\Delta t})T'_I = -2H\Delta xT_a - \frac{\rho C\Delta x^2}{\Delta t}T_I \qquad 3$$

At each time step, the Gauss-Jordan elimination method was applied to solve the triadiagonal matrix.

APPENDIX B - MATHEMATICAL MODEL TO PREDICT TEMPERATURE DISTRIBUTION DURING DIRECTIONAL SOLIDIFICATION

```
C       MATHEMATICAL MODEL TO PREDICT TEMP DISTRIBUTION
C       IN A DIRECTIONALLY SOLIDIFYING Sn-10%Pb ALLOY
        COMMON A(201),B(201),C(201),D(201),TPRIME(201)
        DIMENSION T(201),TN(201),KK(201),TM(201),GRD(200),GHOLD(201
       1,THOLD(200)
        REAL TPOUR,TSOL,TLIQ,TAMB,DELX,DELT,TIMET,DENS,
       1LATENT,CP,K,HT,OT
        TPOUR =226.5
        TSOL=183.0
        TLIQ=215.0
        LATENT=13.5
        HT=0.320E-02
        DENS=7.6999998
        TAMB=20
        DELX=0.05
        DELT=0.50
        OT1=60.0
        CPL=0.0608188
        CPS=0.0614534
        CPM=0.4830111
        TIMET=500.00
        HT1=0.09E-02
        TAMB1=350.0
        OT=5.00000
        DX=0.05
        Z=0.0
        TIME2=0.0
        DO 2 I=1,201
        T(I)=(I-1)/20+TPOUR
        KK(I)=0
        GHOLD(I)=500.0
    2   CONTINUE
        TIME=0.50
C       MATRIX COEFF. A,B,C,D
   90   DO 10 I=1,201
        IF(I.EQ.1) GO TO 20
        IF(I.EQ.201)  GO TO 30
C       MATRIX COEFF. I=2,100
        CALL THERMA (T,I,K)
        CALL SPEC(T,TSOL,TLIQ,I,DELX,DENS,DELT,R,LATENT)
        A(I)=K
        B(I)=-2.0*(K+R)
        C(I)=K
        D(I)=-2.0*R*T(I)
        GO TO 10
C       MATRIX COEFF. I=1
   20   CALL THERMA(T,I,K)
        CALL SPEC(T,TSOL,TLIQ,I,DELX,DENS,DELT,R,LATENT)
        A(I)=0
        B(I)=-(K+HT*DELX+R)
        C(I)=K
```

```
      D(I)=-((HT*TAMB*DELX)+R*T(I))
      GO TO 10
C     MATRIX COEFF. I=101
 30   CALL THERMA(T,I,K)
      CALL SPEC(T,TSOL,TLIQ,I,DELX,DENS,DELT,R,LATENT)
      A(I)=K
      B(I)=-(K+R+HT1*DELX)
      C(I)=0
      D(I)=-R*T(I)-HT1*DELX*TAMB1
      GO TO 10
 10   CONTINUE
      CALL TRIDAG(1,201)
      DO 70 I=1,201
      TN(I)=TPRIME(I)
 70   CONTINUE
      CALL LATEN(I,CPL,CPS,CPM,TN,TLIQ,TSOL,KK,TM)
      DO 97 I=1,201
      T(I)=TM(I)
      KK(I)=KK(I)
 97   CONTINUE
      CALL TIMEX(TIME,OT,I,T,GRD,DX)
      GO TO 1069

      CALL TIMEX(TIME,OT,I,T)
 1070 IF(TIME.GE.20.00.AND.TIME.LE.1600.00)GO TO 1080
      GO TO 1069
 1080 DO 102 I=1,200
      GRD(I)=ABS((T(I)-T(I+1))/DX)
      IF(GRD(I).GE.GHOLD(I))  GO TO 102
      GHOLD(I)=GRD(I)
      THOLD(I)=TIME
 102  CONTINUE
 1069 TIME=TIME+DELT
      IF(TIME.LE.TIMET) GO TO 90
      STOP
      END
C     SUBROUTINE TO CALCULATE THERMAL CONDUCTIVITY
      SUBROUTINE THERMA(T,I,K)
      DIMENSION T(201)
      REAL T,K
      INTEGER I
      IF(T(I).GE.100.0.AND.T(I).LE.225.0)  GO TO 15
      K=-0.000976*T(I)+0.3521
      GO TO 100
 15   K=-0.0000864*T(I)+0.15194
 100  RETURN
      END
C     SUBROUTINE TO CALCULATE SPECIFIC HEAT
      SUBROUTINE SPEC(T,TSOL,TLIQ,I,DELX,DENS,DELT,R,LATENT)
      DIMENSION T(201)
      REAL T,TSOL,TLIQ,DELX,DENS,DELT,R,LATENT
      INTEGER I
      IF(T(I).LT.TLIQ) GO TO 50
      CP=0.0698468-0.0000185*(T(I)+273.0)
```

```
      GO TO 100
 50   IF(T(I).LE.TLIQ.AND.T(I).GE.TSOL)  GO TO 60
      CP=(0.0372398+0.0000531*(T(I)+273.0))
      GO TO 100
 60   CP=(0.0372398+0.0000531*(T(I)+273.0))+(LATENT/(TLIQ-TSOL))
 100  R=DENS*CP*DELX**2/(2*DELT)
      RETURN
      END
C     SUBROUTINE TO CHECK RELEASE OF LATENT HEAT
      SUBROUTINE LATEN(I,CPL,CPS,CPM,TN,TLIQ,TSOL,KK,TM)
      REAL CPL,CPS,CPM,TN,TM,TLIQ,TSOL
      INTEGER I,KK
      DIMENSION TN(201),TM(201),KK(201)
      DO 1000 I=1,201
      IF(TN(I).GT.TLIQ)  GO TO 888
      IF(TN(I).GE.TSOL)  GO TO 1005
      IF(KK(I).EQ.0)     GO TO 1006
      IF(KK(I).EQ.2)     GO TO 1001
C     NODE JUMPS FROM MUSHY TO SOLID
      TM(I)=TSOL-(TSOL-TN(I))*CPM/CPS
      IF(TM(I).GT.TLIQ)   GO TO 1007
      IF(TM(I).LE.TLIQ.AND.TM(I).GE.TSOL) GO TO 1008
      IF(TM(I).LT.TSOL)  GO TO 1009
 1009 KK(I)=2
      GO TO 1000
 1007 KK(I)=0
      GO TO 1000
 1008 KK(I)=1
      GO TO 1000
C     NODE JUMPS FROM LIQUID TO MUSHY
 1005 IF(KK(I).EQ.1)  GO TO 1001
      TM(I)=TLIQ-(TLIQ-TN(I))*CPL/CPM
      IF(TM(I).GT.TLIQ)  GO TO 1010
      IF(TM(I).LE.TLIQ.AND.TM(I).GE.TSOL)  GO TO 1011
      IF(TM(I).LT.TSOL) GO TO 1012
 1012 KK(I)=2
      GO TO 1000
 1010 KK(I)=0
      GO TO 1000
 1011 KK(I)=1
      GO TO 1000
C     NODE JUMPS FROM LIQUID TO SOLID
 1006 TM(I)=TSOL-((TLIQ-TN(I))*CPL-(TLIQ-TSOL)*CPM)/CPS
      IF(TM(I).GT.TLIQ)  GO TO 1015
      IF(TM(I).LE.TLIQ.AND.TM(I).GE.TSOL) GO TO 1016
      IF(TM(I).LT.TSOL) GO TO 1018
 1018 KK(I)=2
      GO TO 1000
 1015 KK(I)=0
      GO TO 1000
 1016 KK(I)=1
      GO TO 1000
 888  KK(I)=0
 1001 TM(I)=TN(I)
```

```
 1000 CONTINUE
      RETURN
      END
C     SUBROUTINE TO SOLVE TRIDIAGONAL MATRIX
      SUBROUTINE TRIDAG(IF,L)
      COMMON A(201),B(201),C(201),D(201),TPRIME(201)
      DIMENSION BETA(201),GAMMA(201)
C     COMPUTE INTERMEDIATE ARRAYS BETA AND GAMMA
      BETA(IF)=B(IF)
      GAMMA(IF)=D(IF)/BETA(IF)
      IFP1=IF+1
      DO 1 I=IFP1,L
      BETA(I)=B(I)-A(I)*C(I-1)/BETA(I-1)
  1   GAMMA(I)=(D(I)-A(I)*GAMMA(I-1))/BETA(I)
C     COMPUTE FINAL SOLUTION VECTOR TPRIME
      TPRIME(L)=GAMMA(L)
      LAST=L-IF
      DO 2 K=1,LAST
      I=L-K
  2   TPRIME(I)=GAMMA(I)-C(I)*TPRIME(I+1)/BETA(I)
      RETURN
      END
      SUBROUTINE TIMEX(TIME,OT,I,T,GRD,DX)
      DIMENSION T(201),GRD(200)
      REAL TIME,OT,T,GRD
      INTEGER I
      IF(TIME.LT.OT) GO TO 201
      WRITE(6,92) TIME
 92   FORMAT(2X,'TIME=',F7.0)
      WRITE(6,93) (T(I),I=1,180,20)
 93   FORMAT(10(2X,F5.1))
      DO 20 I=1,200
      GRD(I)=ABS((T(I)-T(I+1))/DX)
 20   CONTINUE
      WRITE (6,94) TIME
 94   FORMAT(2X,'TIME=',F7.0)
      WRITE (6,95) (GRD(I),I=20,140,20)
 95   FORMAT(8(2X,F7.2))

      OT=OT+5.0
 201  RETURN
      END
C     SUBROUTINE TO CALCULATE RATE OF SOLIDIFICATION
      SUBROUTINE RATEE(I,T,OT1,TIME,TLIQ,DELX,DELT,Z,RATE,TIME2)
      DIMENSION T(201)
      REAL T,OT1,TIME,TLIQ,DELX,DELT,Z,X,RATE
      INTEGER I
      IF (TIME.LT.TIME2)  GO TO 200
      DO 90 I=1,201
      IF(T(1).GT.TLIQ)  GO TO 200
      IF (T(201).LT.TLIQ) GO TO 200
      IF(T(I).GE.TLIQ)  GO TO 100
 90   CONTINUE
 100  TIME2=TIME
```

```
      IF (T(I).EQ.TLIQ)  GO TO 40
      S=(T(I)-T(I-1))/DELX
      Y=(TLIQ-T(I-1))/S
      X=(I-2)*DELX+Y
      GO TO 60
40    X=(I-1)*DELX
60    RATE=(X-Z)/(120.0*DELT)
      IF(TIME.LT.OT1)  GO TO 199
      OT1=OT1+60.0
96    WRITE (5,81) TIME
81    FORMAT(2X,'TIME=',F7.2)
      WRITE (5,82) Z
82    FORMAT (2X,'Z=',F5.2)
      WRITE(5,83) RATE
83    FORMAT(2X,'RATE=',F8.6)
199   Z=X
      TIME2=TIME2+120.0*DELT
200   RETURN
      END
```